MICROFLUIDICS ANALYSER FOR DISSOLVED ORGANIC CARBON

Duarte Nuno Mendonça Costa Moço

Thesis to obtain the Master of Science Degree in:

Chemical Engineering

Supervisor: Prof.ª Dr.ª Susana Isabel Pinheiro Cardoso de Freitas
Co-Supervisor: Prof.ª Dr.ª Teresa Rocha Santos

Examination committee:

ChairPerson: Prof. Dr. Sebastião Manuel Tavares Silva Alves

Supervisor: Prof. Dr. Susana Isabel Pinheiro Cardoso de Freitas

Members of the committee: Dr. Vânia Cristina Henriques Silvério

December 15, 2016

Acknowledgements

This project was executed on the extent of a collaboration between the INESC - Microsystems and Nanotechnology of Lisbon and the Centre of Environmental and Marine Studies at Aveiro University, owing a special thanks to Dr. Prof. Susana Cardoso Isabel Pinheiro Cardoso de Freitas and Prof. Dr. Teresa Rocha Santos for providing me with this opportunity to learn, for the great assistance they provided and for welcoming me into their respective departments.

My gratitude must also be expressed to Dr. Prof: Armando Costa Duarte for all the kindness and sympathy with which he received me in his department and answered my queries.

With the conclusion of this thesis, I must also thank all those who, directly and indirectly, aided me in learning and developing new technical, scientifical and personal skills.

In the first place, I thank Dr. Vânia Silvério for the kindness with which she helped me understand microfluids, teached me how to operate both software and machinery, welding and must important of all, that there is no such thing as a problem, they are only challenges.

I need thank everyone at the Microsystems and Nanotechnology department of the Instituto de Engenharia de Sistemas e Computadores, for providing the occasional tip and overall for creating such a great welcoming atmosphere to work in.

And lastly, I thank my parents, my brother and my girlfriend Catarina Silva for their precious advice, patience, motivation, for showing me that I can accomplish much more than I could ever dream and giving me strength to face my fears and not give in.

Resumo

Devido à vasta panóplia de recções cujo o carbono orgânico dissolvido está envolvido em sistemas de água, é de grande importância ser-se capaz de obter resultados fidedignos a partir das amostras. Um importante aspecto a considerar é a degradação das amostras que ocorre no período de tempo entre colheita da amostra e análise, para minimizar isto, um analisador pequeno, portátil e capaz de análise *in situ* é requerido, que origina necessidade por um analisador mesofluídico. Este projecto estuda a relação entre geometria de mesocanais, velocidades de entrada e a eficiência de mistura para criar um analisador com mesofluídos pequeno e compacto. Várias simulações foram realizadas para simular o escoamento de soluções aquosas em mesocanais e prever a melhor eficiência em mistura, seguido de testes experimentais com estruturas de polimetil-metacrilato (PMMA) dos mesocanais simulados, com uma secção cruzada com 1.0 mm de largura e 0.5 mm de profundidade como dimensões. Este estudo revelou que mesocanais que este estudo designa de canais curvos possuem o melhor potencial em eficiência em mistura, particularmente quando organizados num mesocanal em forma de S, conseguindo atingir mistura completa com o menor caudal de entrada estudado.

Espera-se que os resultados deste estudo, poderão contribuir para o processo miniaturização deste analisador ou outros projectos semelhantes.

Key-words: carbono orgânico dissolvido, simulação mesofluídica, mistura de fluidos, micromaquinação.

Abstract

Due to the vast multitude of reactions which dissolved organic carbon (DOC) is involved with in water systems, it is of great importance to obtain reliable results from the samples. One important aspect to consider is sample degradation occurring in the period between collecting the sample and analysis. To minimize this, a smaller, portable analyser capable of *in situ* analysis is required, which originates the call for a mesofluidic analyser. This project studies the mesochannel geometry, inlet velocity and mixing efficiency relation to create a small compact mesofluidic analyser. Simulations were carried out to understand aqueous solutions dynamics in mesochannels and predict the best mixing efficiency. Those simulated geometries were fabricated with Poly (methyl 2-methylpropenoate) (PMMA) structures, with the following cross-section dimensions: 1.0 mm wide and 0.5 mm deep. We concluded that the curved channels present the best potential in mixing efficiency, particularly when organized in a S-shaped mesochannel.

The results of this study might contribute to the miniaturization process of this analyser and many other similar projects.

Key-words: dissolved organic carbon, mesofluidic simulation, fluid mixing, micromachining.

Index

Figure Index

Table Index

Abbreviation Index

BDOC- biodegradable dissolved organic carbon

CO_2- Carbon dioxide

D_H- Hydraulic diameter

DOC- Dissolved Organic Carbon

DOM- Dissolved Organic Matter

HTO- High Temperature Oxidation

LM- Long Mesochannels

Na_2CO_3- Sodium carbonate

$NaHCO_3$- Sodium bicarbonate

NDIR- Nondispersive Infrared

NOM- Natural Organic Matter

PMMA- Poly(methyl methacrylate)/ Poly(methyl-2-methylpropenoate)

POC- Particulate Organic Carbon

Re- Reynolds number

RGB- Red, Green and Blue

ShM- Short Mesochannels

SM- S-shaped Mesochannels

UM- U-shaped Mesochannels

UV- Ultra Violet

WCO- Wet Chemical Oxidation

1.Introduction

1.1 Natural Organic matter in Water

Natural organic matter (NOM) is a complex mixture of substances which may be classified in two main categories: non-humic and humic substances. Humic substances are defined as organic, biogenic, and heterogenic substances, of natural occurrence, which may, in general, be characterized by the coloration that ranges from yellow to black, of high molecular masses (1–3). Humic substances may be divided into two groups, humic and fulvic acids. Fulvic acids, in general, present lower molecular weights and a higher percentage of carboxyl and hydroxyl groups compared to humic acids (4,5).

NOM in aqueous systems possess various forms include living organisms (biomass), dead particulate materials (debris), and dissolved organic carbon (DOC)(5), such is the size range of natural organic matter, that in seawater, the spectrum of organic structures ranges from small molecules (approximately 10^{-10} m) to whales (approximately 10^{+1} m) (6). As such, NOM is quantifiably divided between particulate organic carbon (POC), and DOC (1,2), the latter being best described, in terms of water content, as: the concentration of carbon remaining in a water sample after all particulate carbon has been removed by filtration and all inorganic carbon has been removed by acidification and sparging. Although the pore size of the filter is a matter open for debate, since there is no specific size stipulated by the scientific community for maximum DOC size, most bibliographical sources that describe DOC and its determination, place pore size for the filter between 0,2 and 1,0 μm (1,2,6–8).

Dissolved organic matter (DOM) is operationally defined as the organic material that passes a filter, which after acidification and sparging, is quantified as DOC, includes a wide range of constituents from truly dissolved, small molecules like acetate, to macromolecules such as humic acids, to submicro-meter-sized particles such as viruses (8). As such, in aquatic ecosystems, the DOC sources may be characterized as allochthonous organic matter, organic matter produced outside the aquatic system entering it by terrestrial via, and autochthonous organic matter, produced inside the aquatic system, derived from the biota (algae, bacteria, macrophytes)(5).

Environmental scientists are increasingly emphasizing the geochemical and ecological roles of organic matter in aquatic ecosystems, since organic matter in aqueous systems often controls geochemical processes by acting as a proton donor or acceptor and as a pH buffer, by affecting the transport and degradation of pollutants, and by participating in mineral dissolution and precipitation reactions (5,9). As such here is listed some of the various ways organic matter, mainly DOC, impacts aquatic ecosystems biodegradable dissolved organic carbon (BDOC) is the fraction of the DOC which can be metabolized by bacteria within a period of a few days to a few months, removal of this form of carbon is of particular importance for the water treatment industry because BDOC reaching the distribution system can be responsible for bacterial regrowth; DOC is a reactant in aquatic photochemical reactions (10); DOC alters aquatic ecosystem chemistries by contributing to acidification of freshwater systems, particularly those of low alkalinity and weakly buffered; through chelation of metals, DOC forms water-soluble complexes with trace metals, which affects mobilization and speciation of metals in solution

allowing them to be absorbed by aquatic organisms and entering the food chain; DOC water content affects the solubilisation of hydrocarbons (11); DOC is involved in the formation of particulate matter (12), in other words, in the formation of POC; also POC, in high concentrations alters water colour, which affects light penetration, which, in turn, affects plants and other ecosystem's phototrophs that require light to subsist. (1,2,13–17)

Both POC and DOC are important components in the carbon cycle, the biogeochemical cycle of carbon exchange between biosphere, pedosphere, geosphere, hydrosphere and atmosphere driven by solar or geothermal energy and operating on time-scales of microseconds to eons. Studying the biogeochemical cycle of carbon, and other biogeochemical cycles, is the cornerstone of understanding the fluxes and feedback mechanisms that help maintain environmental conditions within the narrow bounds necessary for life to exist. An integral part of this research on the carbon cycle, is quantifying the water (whether fresh water or saltwater) content of DOC and its sources. A convenient means of determining the overall amounts and fluxes of organic compounds in natural cycles is to use reduced carbon as a general tracer. In addition to being the major elemental component of organic matter, reduced carbon is easily quantified by combustion to CO_2 and can be readily separated from coexisting acid-volatile carbonates. The relative abundances of the stable (^{13}C and ^{12}C) and radioactive isotopes of carbon also provide a useful imbedded tracer and clock, respectively. (1,2,18)

1.2 DOC determination

To quantify DOC water content, there are several techniques divided into two major categories according to oxidation method:

- **High Temperature Oxidation (HTO)**: it involves conversion of inorganic carbon to dissolved CO_2, and purging this from the sample, the remaining (organic) carbon is then oxidized at a high temperature (680-1100ºC) to CO_2, tipically aided by metallic catalyst or quartz beads, which can then be detected by the instrument's nondispersive infrared (NDIR) sensor. (1,19–21)
- **Wet Chemical Oxidation (WCO):** involves the same initial steps as HTO, up until after the purge of inorganic CO_2, when the remaining (organic) carbon is then oxidized by chemical oxidation with an oxidant (often persulfate) and/or by photo oxidation with UV irradiation which can be detected by the NDIR sensor. (1,19,21–24)

Although these methods are based on the same modus operandi: conversion of inorganic carbon in CO_2, purging inorganic CO_2, oxidation of organic matter and measuring organic CO_2; a lot of discussion in the scientific community revolves around them. The reason for this debate, is best summarised by Wangersky in his work "The determination of dissolved organic carbon in sea" (1981) (25) in which is stated the usefulness of being able to measure DOC content with good precision and the difficulties in finding appropriate oxidation method and a good CO_2 determination technique, especially if the equipment is intended to work at sea. Central to this problem is the debate of which of these methods is the most efficient by detecting the most DOC content in water. Reports of elevated DOC concentrations being measured with HTO techniques when compared with concentrations measured with WCO techniques (26–28), yet, other works failed to show such differences ((29,30)). Several reviews and

further works performed on the matter of determination of DOC, postulate that these discrepancies might not be indicative of differences in efficiency, being most likely caused by a number of reasons including: measurement of different DOC pools; poor working conditions; contamination; unaccounted blanks associated with HTC techniques; and regional and seasonal differences in DOC (21,25,31–37). Also, part of the problem with the current DOC determination techniques, they are susceptible to salt interference when analysing seawater.

Despite discrepancies might not be correlated to different methodology efficiency, some works claim HTO method to be preferable to WCO, on the grounds of full oxidation (combustion) of organic material is more probable in the former case than in the later (24), also HTO procedure is compatible for simultaneous determination of DOC and Total Dissolved Nitrogen in the same sample in a single injection through coupling of commercial instruments for the DOC analyser and a nitrogen chemiluminescence detector (20). However, HTO technique has several handicaps and limitations, for instance: since it requires a preliminary drying step, there is a maximum limit to the volume of the sample to be analysed, or the sample will not fully dry; due to being more sensitive in CO_2 detection, this method is more susceptible to contamination, as a exemplified in the work of Cauwet, "Automatic determination of dissolved organic carbon in seawater in the sub-ppm range" (34), where a 0.1µg carbon in a 100-µL sample is equivalent to a 1 mgL^{-1} deviation; also sodium chloride can be responsible for two types of mistake: the fast drying of the sample can provoke the ejection of small particles; and the partial volatilization of NaC1 at the usual temperature (700-- 800°C) and its further deposition on the combustion tube walls which translates in poor reproducibility (24,34).

As for WCO method, due to this technique's proneness to incomplete conversion of the oxidation reaction of organic matter, several sources report of WCO analysers yielding a lower DOC concentration when compared to HTO analysers and many other works favouring HTO over WCO method. Chemical oxidation with persulphate as an oxidant, requires high temperature and a high-reagent concentration to produce reliable results. As for photo oxidation through UV irradiation, it was demonstrated to be unable to oxidise some organic compounds completely, except with very energetic lamps (1000 W). However the combination of these two oxidation methods seems to be able to solve most of these problems, including salt interference with seawater samples, caused by the low content in organic carbon compared with the high salt concentration and the subsequent oxidation of the chloride to chlorine in persulphate (34,38), this interference can be overcome by increasing digestion time, by diluting seawater samples or by significantly increasing the concentration of persulfate, this last option is the most advantageous since it still allows short reaction times to be employed and avoids errors or contamination from the dilution of sample (35). This capacity of handling high salt concentration samples is what makes the WCO the most popular choice despite the potential lower results compared to the HTO method.

In the end both categories of techniques have their own limitations and shortcomings, one and foremost, the controversial variability between methods with no clear answer as to which is the most precise and efficient, as such, the most effective means of assessing the variability between the different methodologies is still through direct intercomparison experiments, however since few laboratories can afford two DOC analysers, and so some compromise instrument is usually sought (25,35), specially taking in consideration sample composition and place of analysis.

1.3 Focus

The present thesis was originated from a collaboration between the Centre of Environmental and Marine Studies at Aveiro University (CESAM-UA) and the Microsystems and Nanotechnology department of the Instituto de Engenharia de Sistemas e Computadores (INESC-MN). The theme was born out of frequent analysis of the water samples from estuary of the river Vouga, located near the city of Aveiro, performed by by the team in CESAM and their need for a smaller, portable device capable of shipboard analysis *in situ*, in order to avert sample degradation during transportation from the collection site to the lab. As such the focus of the present thesis, is describing the procedure behind the development in mesofluidic format of an analyser of DOC in water with the same analysing process of a SKALAR™ analyser of DOC as described in the paper "The Assembling and Application of an Automated Segmented Flow Analyzer for the Determination of Dissolved Organic Carbon Based on UV-Persulphate Oxidation" (Lopes et al.) (39).

1.4 SKALAR™ Dissolved Organic Carbon Analyser

To understand the objectives of this thesis and decisions taken to accomplished said objectives, it is relevant to understand the operating process behind the SKALAR™ DOC analyser, which this project aimed to emulate in mesofluidics. According to the article (39), the analyser, is capable of detecting DOC, by converting DOM into CO_2 through UV-persulphate oxidation, and later measuring the discolouring of a phenolphthalein solution due to its concentration of carbon dioxide.

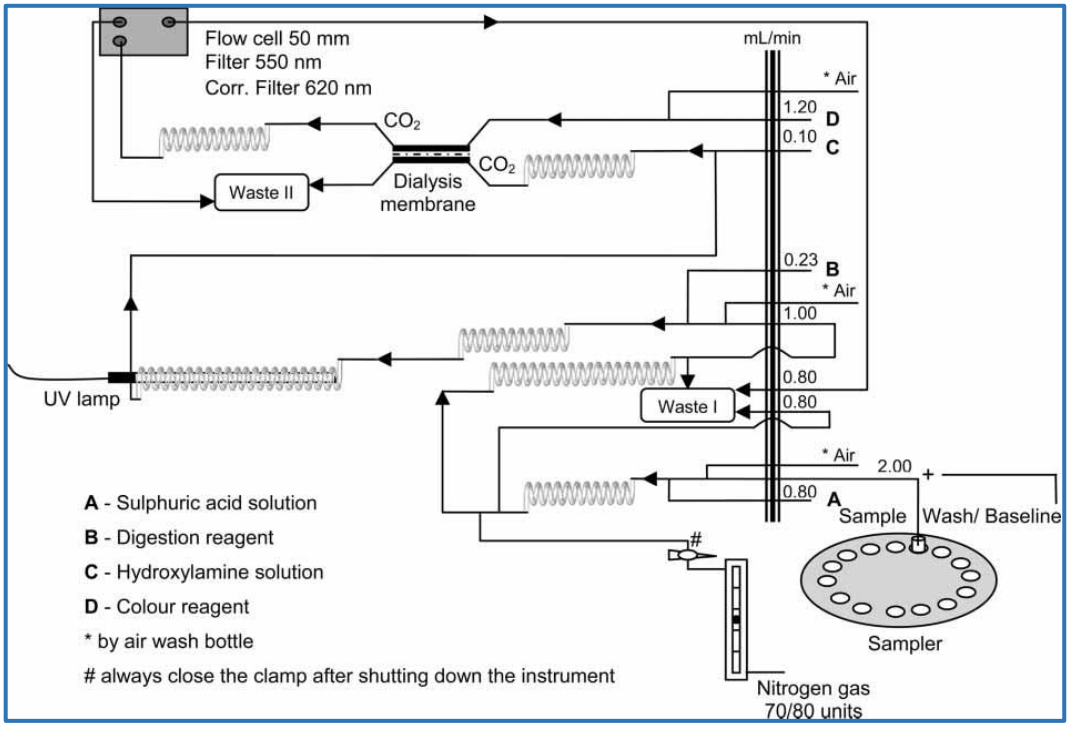

Figure 1: Flow diagram for dissolved organic carbon (DOC) analysis. (39) **Indicated in the lower left corner with (A, B, C and D) are all the reagents used in the process**

As described in (39), where the volumes described correspond to the amount of reagents and solutions necessary to process 1 mL of sample, the process begins with the removal of impurities and possible CO_2 from inorganic sources, after the sample is pumped with a peristaltic pump into the apparatus, it comes into contact with a sulphuric acid solution (Reagent A-Figure 1, 1.68 mL/L) and is mixed in the first mixing coil with the purpose of producing carbon dioxide from inorganic matter.

To remove this CO_2, the solution is sparged with nitrogen (70/80 units+19 liter/hour) to remove inorganic carbon and passes through a second mixing coil, which at the end, gaseous phase is removed and with it the inorganic carbon. As it is now, the only remaining carbon inside the solution is from organic source, which prevents interferences from inorganic matter.

A digestion reagent (Reagent B- Figure 1), prepared by dissolving 3 g of potassium persulphate and 8.5 g of sodium tetra-borate in 250mL of Milli-Q water, is added to the solution before entering the third mixing coil, and following it, the mixture is irradiated in a digestion coil with a UV lamp (wavelength 185 nm). It is in this digestion coil that the organic matter is converted into CO_2. After organic matter oxidation, a hydroxylamine solution (Reagent C- Figure 1), prepared by dissolving 10 g of hydroxyl ammonium chloride in 100mL of Milli-Q water and adding 2mL of sulphuric acid (97%) and 0.5mL of Triton X-100 (10%) is added to the sample before entering the fourth mixing coil. Afterwards, the mixture enters the dialyser composed of two overlapping channels separated by a semi-permeable membrane through which carbon dioxide can pass by diffusion. The sample flows through one of the channels, the CO_2 diffuses through the membrane into the other channel, where a weakly buffered phenolphthalein indicator (Reagent D- Figure 1) is flowing in counter current to the sample.

The rest of the sample and reagents are removed from the apparatus to waste. The phenolphthalein indicator is prepared by adding adding 0.3mL of a buffer solution (2.65 g of Na_2CO_3 and 2.10 g of $NaHCO_3$ in 100mL of Milli-Q water), 0.5mL of Triton X-100 (10%), and 0.3mL of 1% phenolphthalein in a 500mL of mixture (1/9 v/v) of ethanol and distillate water. This indicator colour intensity decreases due to a pH change induced by the presence CO_2, this decrease is proportional to the CO_2 concentration.

The colour intensity is measured at 540 nm with correction filter of 650 nm in a flow cell of 5 cm. It is important to mention that this apparatus works by pumping small alternating doses of sample solution and wash solution (Milli-Q water) to avoid accumulation of residue inside the tubes, thus avoid contamination of later samples.

On the early phase of this project, the laboratory of the Chemistry department of Aveiro University was visited for a first hand study of the current SKALAR™ DOC analyser, the process and the required equipment. This visit yielded several pictures of the SKALAR™ analyser complement the previous process description.

To better understand the scope of this thesis, the analyser was divided into 4 units, which were developed separately: the sampler, the interface, the optical unit and the chemical unit (39)

1) **Sampler** - part of the device which will harbour the samples, washing solution and other solutions, and a pump to pump these solutions into the chemical unit.

2) **Interface -** computational component, responsible for connecting the computer to the analyser, controlling the pump and other equipment of the analyser and converting the signals received by the optical unit into data.
3) **Optical unit -** section holding all the components necessary for determining CO_2 concentration in a phenolphthalein solution: lamp, wavelength filter, light detector, and electrical components to power up the lamp and the detector.
4) **Chemical unit -** an assembly of channels and mixing coils combined with UV lamp digester and a dialyser, where the sample will be treated, to remove inorganic impurities, convert organic matter into CO_2 and extract it to be analysed in the optical unit.

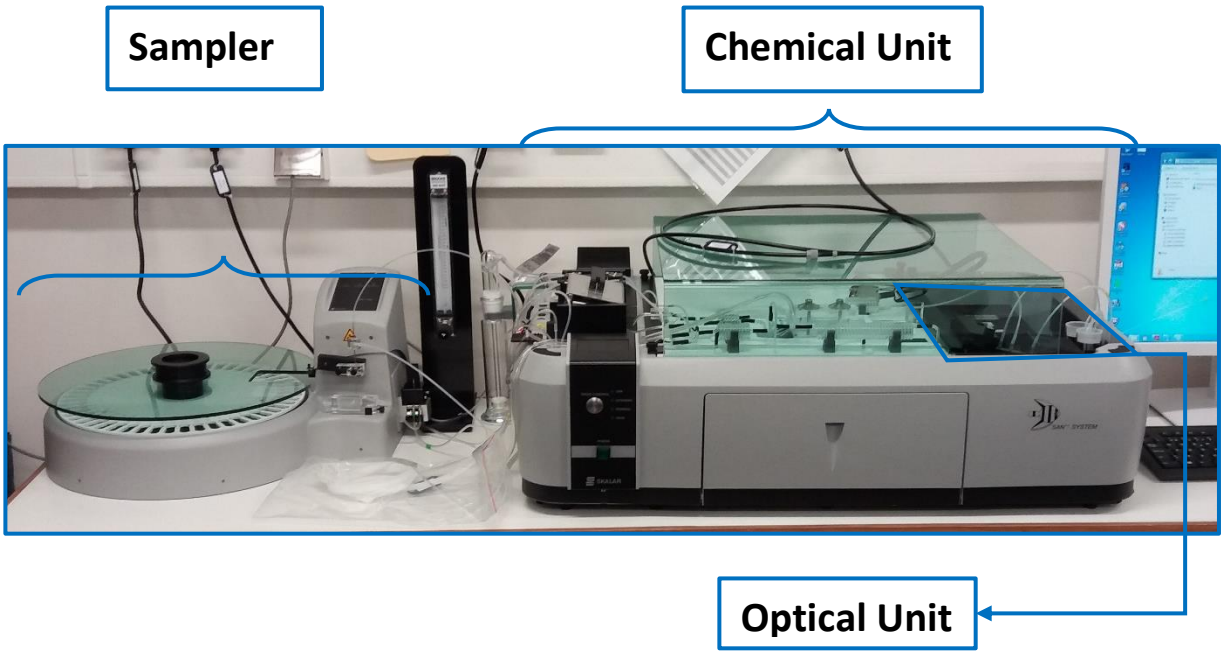

Figure 2 SKALAR™ analyser employed in DOC determination in the Chemistry laboratories of Aveiro University

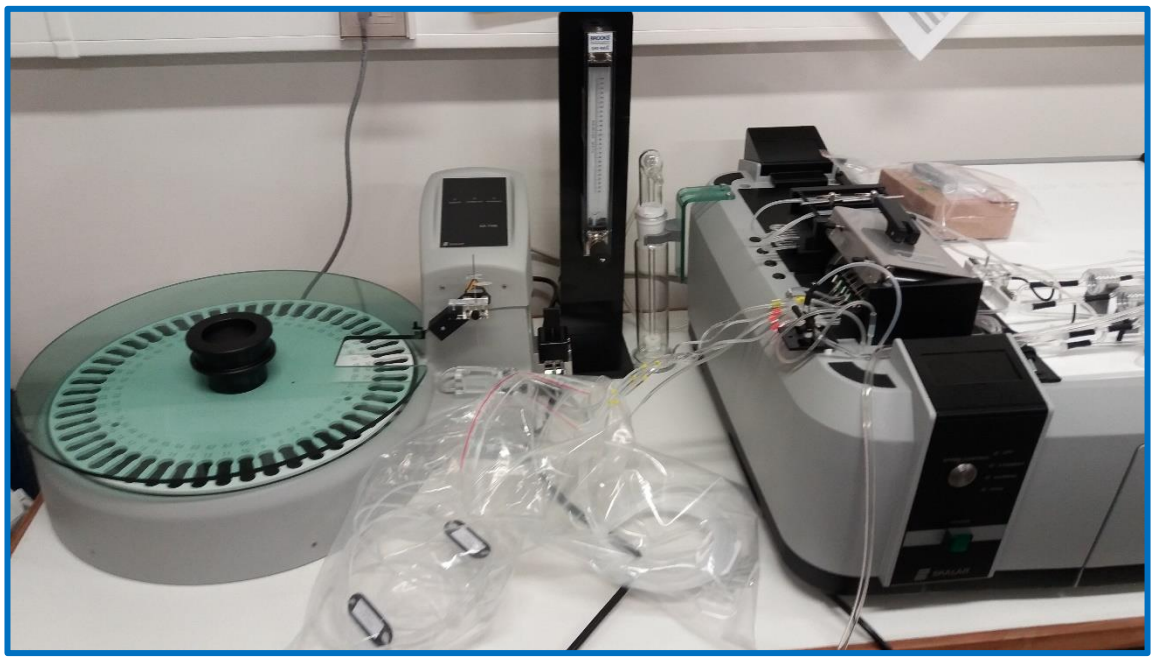

Figure 3 Close-up of the sampler and peristaltic pump

Figure 4 Interface of the analyser

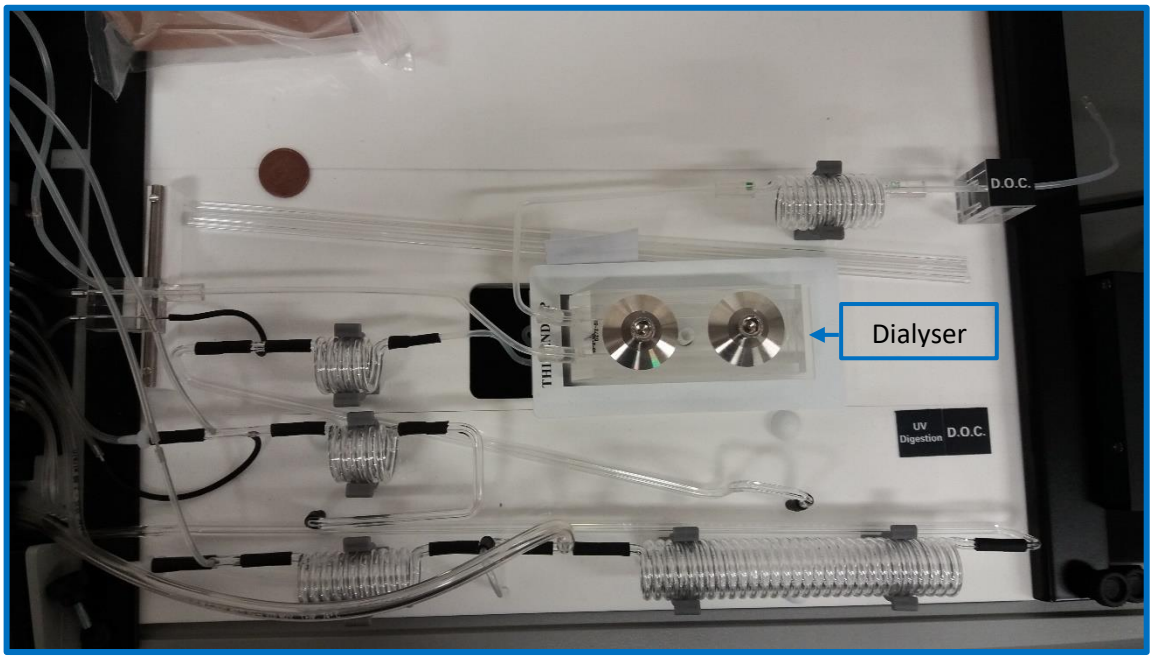

Figure 5 Top view of the tubbing, mixing coils and the dialyser in the chemical unit. UV lamp resides directly underneath this platform, inside the chemical unit.

Figure 6 Close-up of the optical unit of the analyser

1.5 Requirements

Although in the paper (39) its already described an analyser with the process described as "portable" and capable of shipboard analysis, in reality, the SKALAR™ analyser fully assembled is a bulky machine with several isolated instruments and pieces connected only by sillicon tubbing and cables, also difficulting portability is the fact that several parts of the apparatus are delicate, such as quartz mixing coils in the needle and revolving arm in the sampler, and may not be sturdy enough to whitstand frequent trips for in situs analysis, as shown in the previous subchapter. As such, the mesofluidic analyser has a set of requirements to be met in order to be of proper use to the investigators team of CESAM. Firstly, the final device show be small enough to be carried by car from the laboratory to Vouga river, and be loaded into and unloaded from a small boat. Secondly, it should easily handled inside the small boat, as such, have a very simple assembly, with the least amount of individual parts as possible, to facility handling, optimum scenario would be only 2 parts: the analyser and a portable computer, however, optimum scenario is highly improbable of achieving since reagent recipients have to be taken into consideration. Also, as an added requirement, is changing the current process from segmented flow to continuos flow by removing the air inlet, this will simplify the new process and eliminate the equipment necessary to prevent contamination of the sample through air contact.

The present thesis originally set out to tackle the development each of the four units of the analyser individually in a first attempt to reduce their size before attempting to join them to eliminate individual movable parts, but given the approximately one year period allocated to research, test and write the present thesis, all these units could not be encompassed, and thus, this thesis focus on the development of the chemical unit, since it is more within the field of knowledge of chemical engineering, and the bulkiest unit.

2. COMSOL Multiphysics 5.0 Simulations

A mesochannel was designed and simulated using COMSOL Multyphysics 5.0 to ascertain their mixing properties. The simulations were carried out on a similar fashion as the simulations described by the paper "Computational Analysis for Mixing of Fluids Flowing through Micro-Channels of Different Geometries" by Das et al.(40). The cinditions ae futher described of the following sub-chapters.

2.1 Modelling

A wide variety of geometries were simulated, varying parameters such as angle of joining of two channels, size and number of obstacles, to determine how they affect mixing.

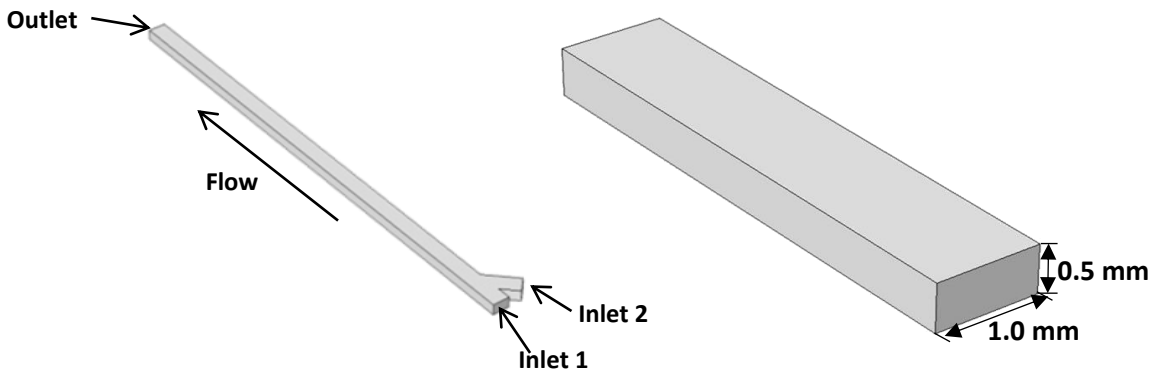

Figure 7: Geometry used for the mesochannels and the dimensions of channels

The mesochannels have a cross section of 1mm width and 0.5 mm depth; the obstacles are designed to also have 0.5mm height. Inlet velocity of both inlets was set at 0.1 m/s and outlet relative pressure was set at 0 Pa.

For this purpose, the simulations carried out for the Generation-0 mesochannels were divided in 4 types, according to design:

a) Straight channels
b) Square pillars (1-2) formation channels
c) Square pillars (1-1) formation channels
d) Curved channels

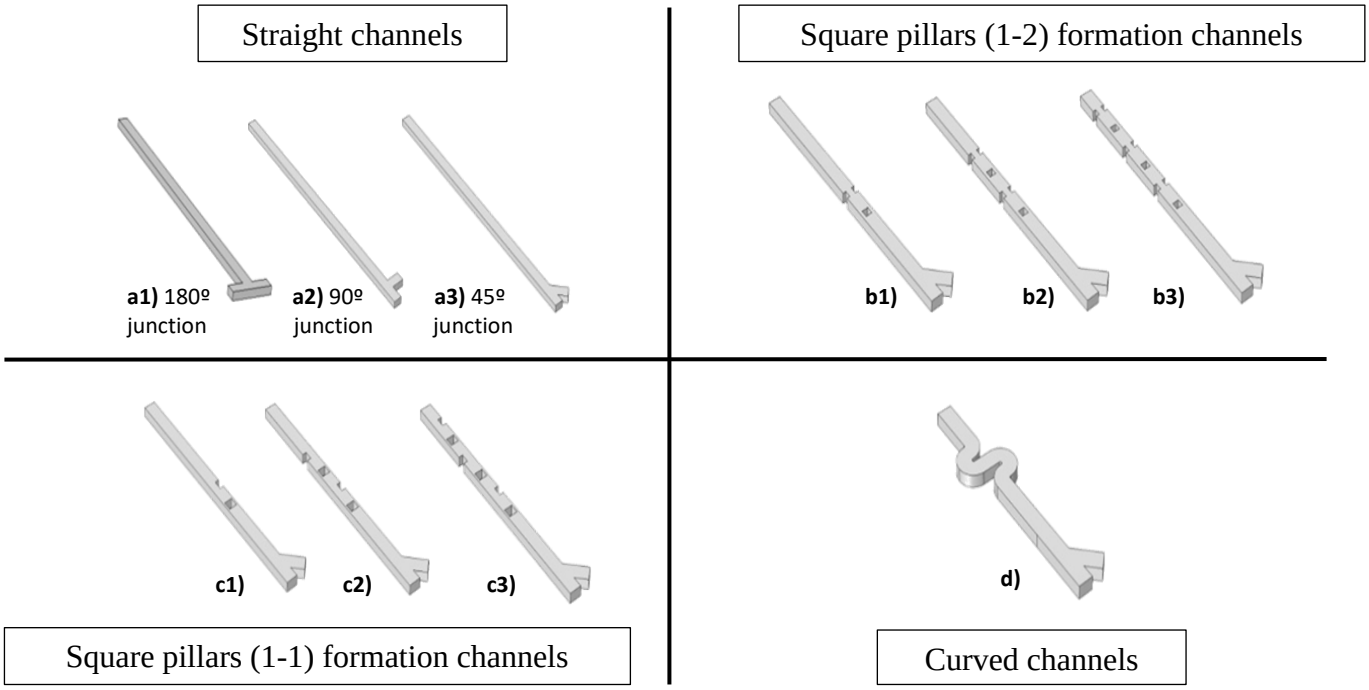

Figure 8: (a) Straight Mesochannels with 180 degree junction, 90 degree junction and 45 degree junction (1,2 and 3, respectively); (b) Straight Mesochannels with square pillars 3, 6 and 9 pillars (1,2 and 3, respectively); (c) Straight Mesochannels with square pillars 2, 4 and 6 pillars (1,2 and 3, respectively); (d) Curved Mesochannels.

2.2 Meshing

For analysis, the models were imported to COMSOL software and meshing was performed using structured meshing method and by selecting normal element size.

2.3 Simulation

The computational analysis of all the micro-channels was performed using COMSOL Multiphysics software, the full procedure is described in the Attachments A. For the flow analysis, 'Laminar flow' model was selected under 'Single Phase Fluid Flow' of model wizard. As this was a mixing based problem, 'Transport of Diluted Species' model was selected under 'Chemical Species Transport' of model wizard and to solve the problem 'Stationary Solution' was considered. The inlets are placed at the bottom of the mesochannel structure, before the junction and the outlet is placed at the other end of the mesochannel.

Since all, but two, of the fluids applied in the SKALAR™ analyser are water based solutions with low concentrations of solutes, for simulations purposes all fluids were assumed to possess the same properties as liquid

water at ambient temperature, using the specifications from the material library of the COMSOL Multiphysics 5.0. The two other fluids applied in the original analyser are air, for flow segmentation, which this new analyser is trying to avert, and nitrogen gas, to extract dissolved CO_2 from inorganic sources residing in the sample.

Since the SKALAR™ analyser has no form of temperature control for the samples, it was considered that the analyser operates at room temperature (T=20ºC=293.15K), COMSOL Multiphysic adjusted, according to the temperature selected, the density of water (ρ) as 998.21 kg/m3 and dynamic viscosity (μ) as 1.0016 mPa.s.

The inlet velocity was calculated as follows:

It was assumed that the flow in both the mesochannels and in the SKALAR™ analyser would operate in the same regime, as such, the Reynolds number (Re) is assumed to be the same for both instances.

$$Re = \frac{\rho . u . D}{\mu} \qquad Eq.(1)$$

It is known, through the description of the equipment in the SKALAR™ analyser's manual, that the inner diameter of the tubbing is 1.5 mm and through the article (39), that the maximum flow rate in the analyser is 2.0 mL/min.

As such Reynolds calculated through the eq (1) and the following data, displayed in Table (1).

Reynolds number, Re	**28.20**
Inner Diameter, D (m)	1.50×10^{-3}
Cross section area of the tube (m^2)	1.77×10^{-6}
Inlet velocity, u (m/s)	1.89×10^{-2}
Flow rate, Q (mL/min)	2.00
Dynamic viscosity at 20ºC, μ (Pa.s)	1.00×10^{-3}
Density at 20ºC, ρ (Kg/ m^3)	998.21

Table 1: Flow properties in the SKALAR™ analyser's tubes

The mesochannels were designed with a with 0.5 mm of height (h) and 1,0 mm of width (w). The hydraulic diameter, D_H, was calculated through the following equation:

$$D_H = \frac{4 \cdot Area}{Perimeter} \leftrightarrow D_{H_{rectangle}} = \frac{4 \cdot h \cdot w}{2(h+w)} = \frac{2 \cdot h \cdot w}{(h+w)} \qquad Eq.(2)$$

Following the calculation of the hydraulic diameter, inlet velocity and flow rate can be determined with Eq. (1) and is displayed in Table 2.

Reynolds number, Re	*28.20*
Hydraulic Diameter, D_H (m)	6.67×10^{-4}
Cross section area of the tube (m^2)	5.00×10^{-7}
Inlet velocity, u (m/s)	**4.24×10^{-2}**
Flow rate, Q (mL/min)	**1.27**
Dynamic viscosity at 20ºC, μ (Pa.s)	1.00×10^{-3}
Density at 20ºC, ρ (Kg/ m^3)	998.21

Table 2: Flow properties in the mesochannels

The simulation was performed with the same inlet velocities (for both inlets) of 4.24×10^{-2} m/s, the outlet was kept at atmospheric pressure, initial values state no velocity field. The channel walls were assigned to *no slip conditions*. On the other hand, a concentration of particles was assigned to both inlets, *convective flux* was imposed at outlet and *no flux conditions* was assigned to walls. No specific material as selected in the diffusion to run the simulation, since the analyser will require to mix several aqueous solutions with various compounds, so for testing we only specified that the concentrations for the inlet 1 and 2 would be as 0 mol/m^3 and 100 mol/m^3, respectively, therefore if full mixing is achieved the overall concentration would be 50 mol/m^3.

Width (μm)	*1000*
Depth (μm)	500
Hydraulic Diameter., Dh (μm)	666.67
Area, A (m^2)	5.00×10^{-7}
Flow rate, Q (mL/min)	**1.27**
Inlet Velocity, V (m/s)	**4.24×10^{-2}**
Reynolds number, Re	28.20

Table 3: Input parameters used for simulation of the mesochannels

2.3.1 Simulation of Generation-0 Mesochannels

2.3.1.1 Simulation of Straight channels

The straight micro-channel was tested to determine if a good level of mixing could be achieved with simple structures by mere diffusion and what effect the junction angle between two inlets will have on mixing.

The junction angles tested were 45, 90 and 180 degrees formed by the two inlets.

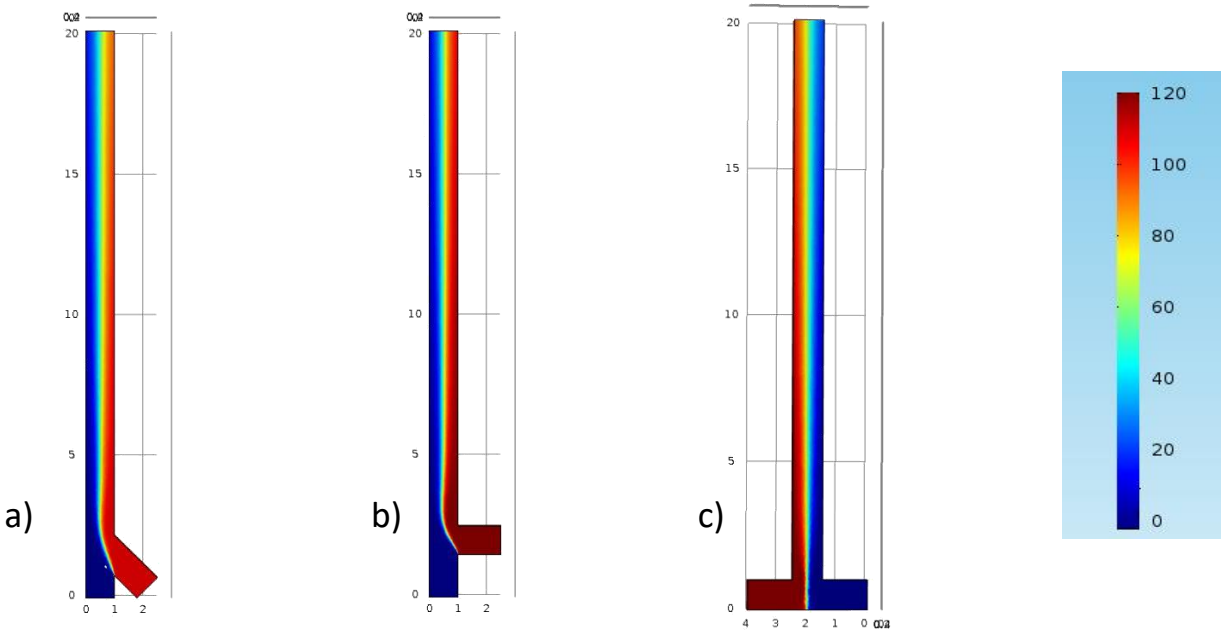

Figure 9: Concentration of the straight channels, a) with 45º, b) with 90º and c) with 180º angle between inlet. The mesochannels have 20 mm of length. Scale represents a colour code for the concentration gradient in mol/m^3. View of a XY plane crossing the middle of the mesochannel

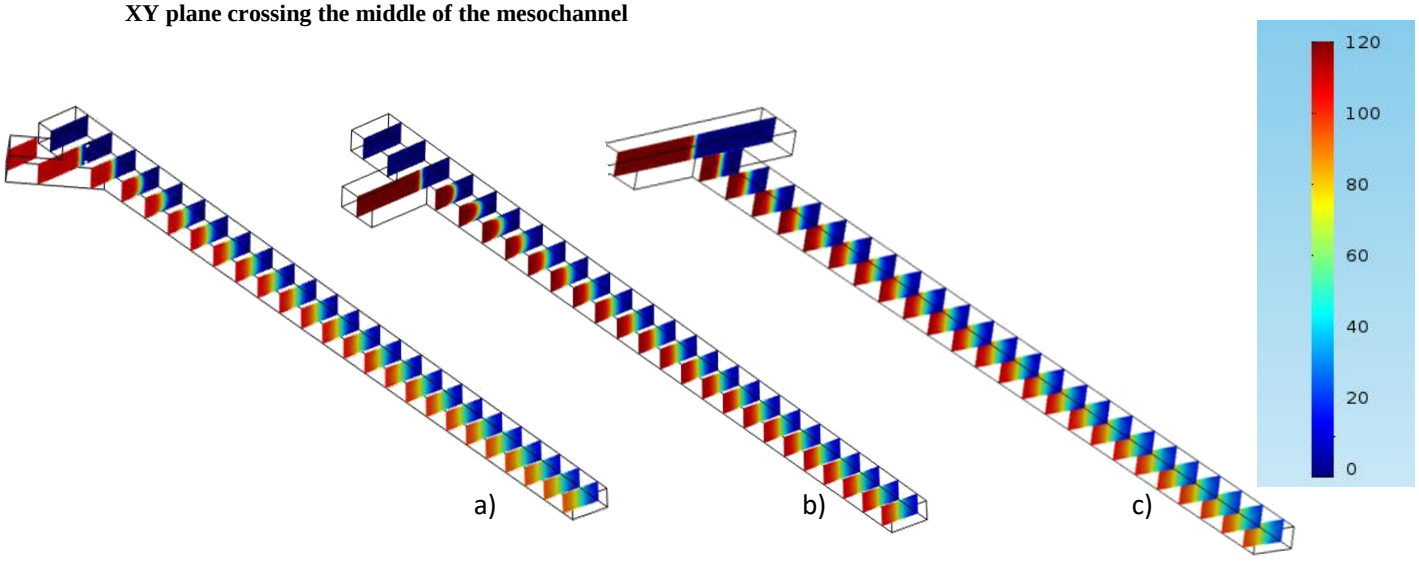

Figure 10 Concentration of the straight channels, a) with 45º, b) with 90º and c) with 180º angle between inlet. The mesochannels have 20 mm of length. Scale represents a colour code for the concentration gradient in mol/m3. View of 25 XZ planes showing several cross-sections of the mesochannel

As it can be seen in Figures 12 and 13, the junction angle formed has very little impact in the degree of mixing, so later designs possess a 45 degree angle which allows a better organisation of the inlets, making it possible for the design to have all sample and reagents inlets in the same side.

2.3.1.2 Simulation of Square pillars (1-1) formation channels

This design was chosen to test if mixing could be easily reached with simple square shaped obstacles to force fluid to move transversally inside the mesochannels.

For the design, the straight section of the mesochannel is alternated between square obstacles in the centre of the mesochannel and half a square pillar attached to the side (alternating between sides) of the mesochannel, as represented in Figure 11, the obstacles' centres are set 2 mm apart of each other in the direction of the channel.

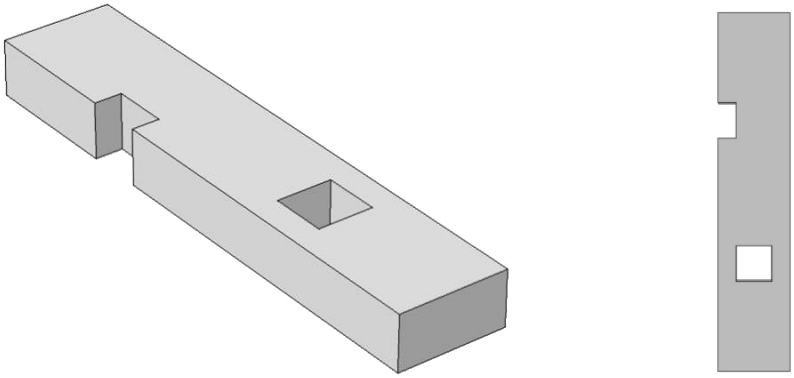

Figure 11 Visual representation of the square pillars in a (1-1) formation, in grey represents the volume that will be occupied by fluid. Isometric representation on the left and top view on the right

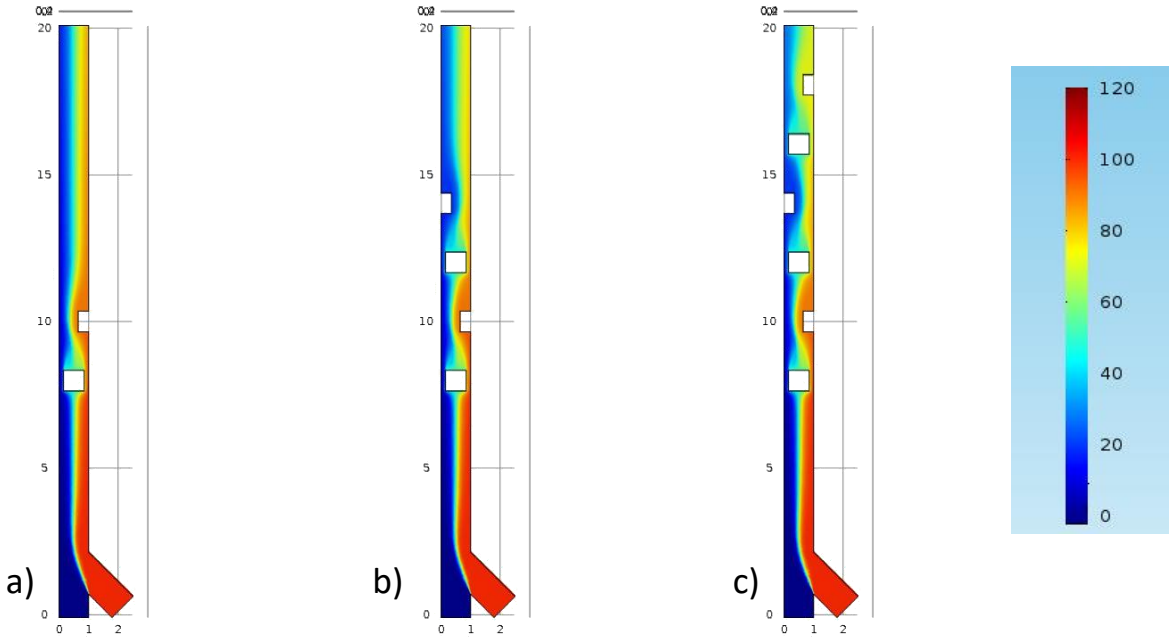

Figure 12: Concentration of the 0.7 mm square pillars (1-1) formation mesochannels, a) with 2 pillars, b) with 4 pillars and c) with 6 pillars. The mesochannels have 20 mm of length. Scale represents a colour code for the concentration gradient in mol/m^3. View of a XY plane crossing the middle of the mesochannel

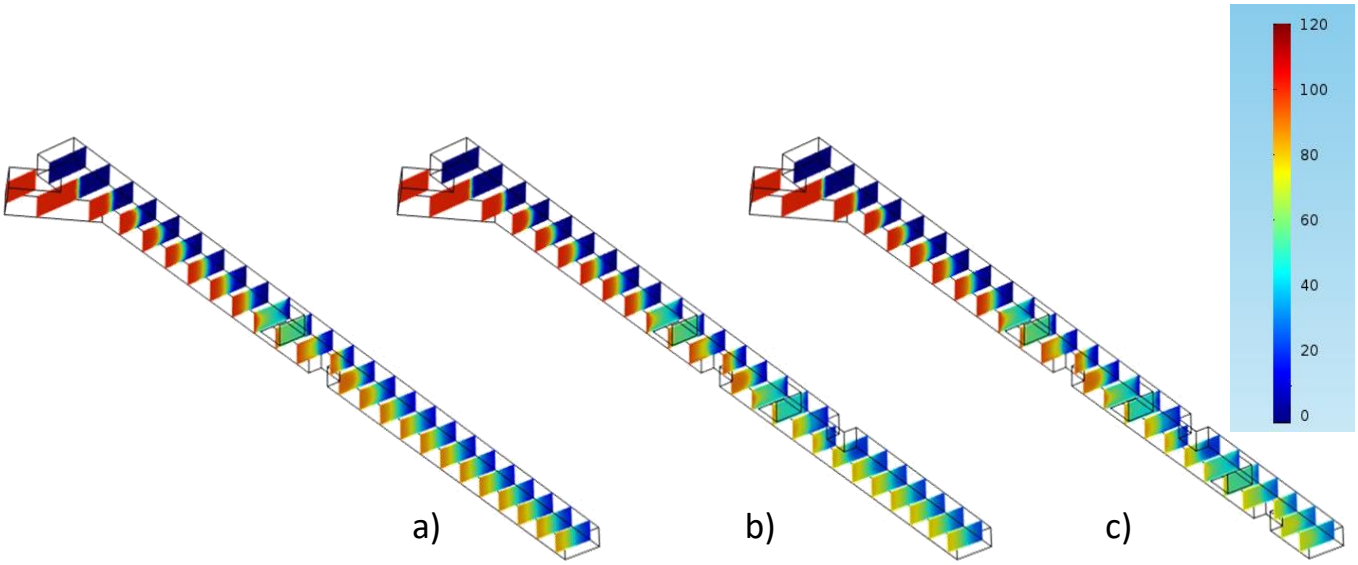

Figure 13 Concentration of the 0.7 mm square pillars (1-1) formation mesochannels, a) with 2 pillars, b) with 4 pillars and c) with 6 pillars. The mesochannels have 20 mm of length. Scale represents a colour code for the concentration gradient in mol/m^3. View of 25 XZ planes showing several cross-sections of the mesochannel

Figure 12 and 13, shows that with a greater the number of obstacles, its possible to achieve a significantly better the mixing than the channels with other channels with less or no obstacles at all like the Straight mesochannels, this happens because the obstacles disrupts the flow of the fluid, forcing high concentration fluid to move to the lower concentration side of the mesochannel and low concentration fluid move to higher concentration side of the mesochannel.

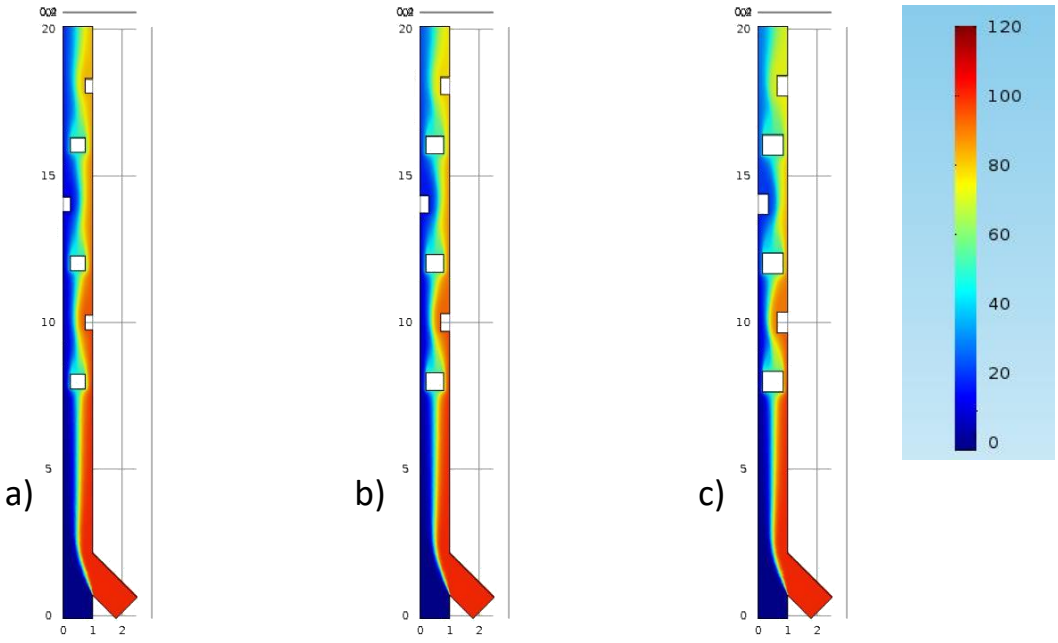

Figure 14: Concentration in square pillars (1-1) formation mesochannels with the following size of pillars: a)0.5mm side; b) 0.6mm side; and c) 0.7mm side. The mesochannels have 20 mm of length. Scale represents a colour code for the concentration gradient in mol/m^3. View of a XY plane crossing the middle of the mesochannel

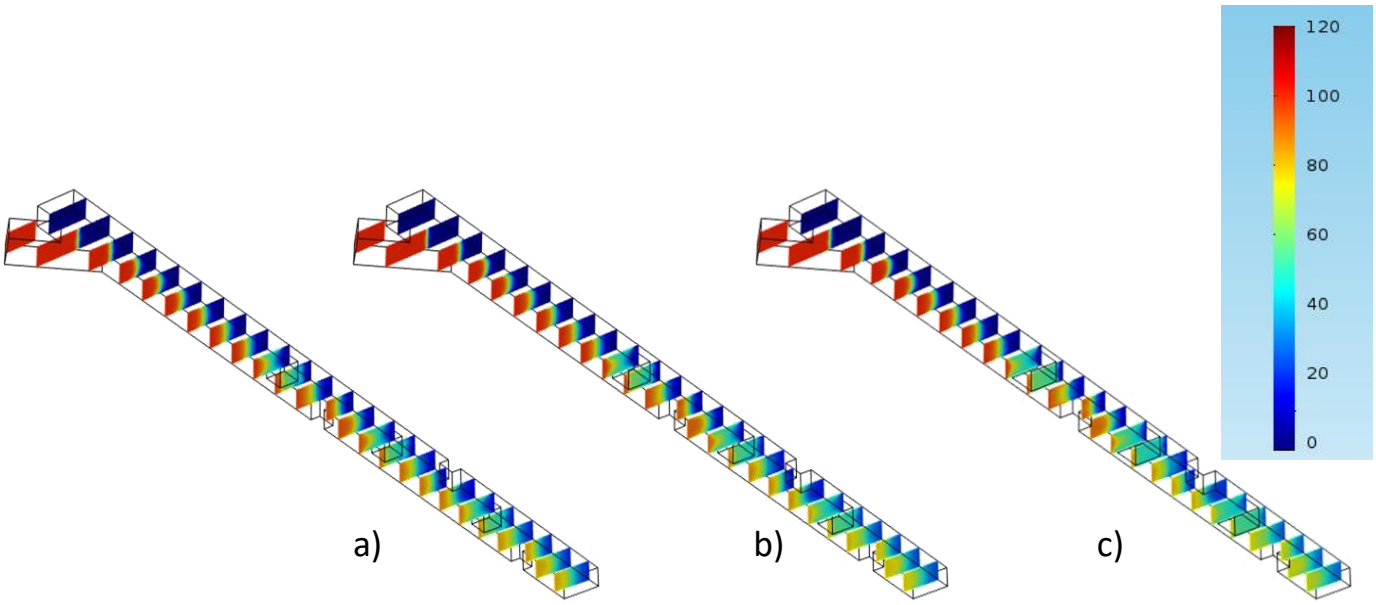

Figure 15 Concentration in square pillars (1-1) formation mesochannels with the following size of pillars: a)0.5mm side; b) 0.6mm side; and c) 0.7mm side. The mesochannels have 20 mm of length. Scale represents a colour code for the concentration gradient in mol/m^3. View of 25 XZ planes showing several cross-sections of the mesochannel

Figures 14 and 15, shows that with bigger obstacles is possible to achieve better the mixing, with the 0.7 mm pillars showing the most promising results. However, this design poses several problems, further detailed in chapter 3.1, one being that, tampering with the size of these obstacles have some limitations, since thinner pillars can be easily broken off, even during the process of fabrication, and wider pillars may lead to obstructions that completely stop the flow.

2.3.1.3 Simulation of Square pillars (1-2) formation channels

Following a design similar to the one employed in chapter 2.3.1.2, with extra obstacles to increase fluid flow disruption in an attempt to further increase mixing.

For the design, the straight section of the mesochannel is alternated between square obstacles in the centre and half a square pillar attached to both sides of the mesochannel, as represented in Figure 16, the obstacles' centres are set 2 mm apart of each other in the direction of the channel.

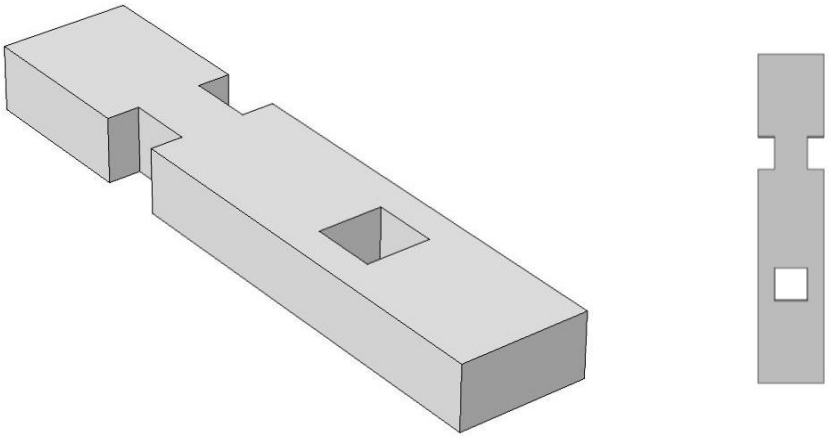

Figure 16 Visual representation of the square pillars in a (1-1) formation, in grey represents the volume that will be occupied by fluid. Isometric representation on the left and top view on the right

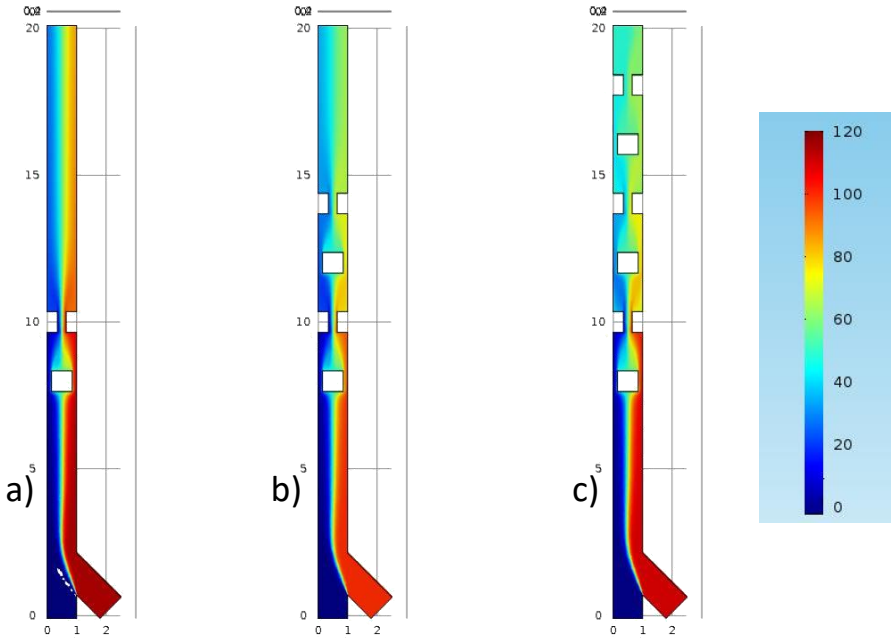

Figure 17: Concentration of the 0.7 mm square pillars (1-2) formation mesochannels, a) with 3 pillars, b) with 6 pillars and c) with 9 pillars. The mesochannels have 20 mm of length. Scale represents a colour code for the concentration gradient in mol/m^3. View of a XY plane crossing the middle of the mesochannel

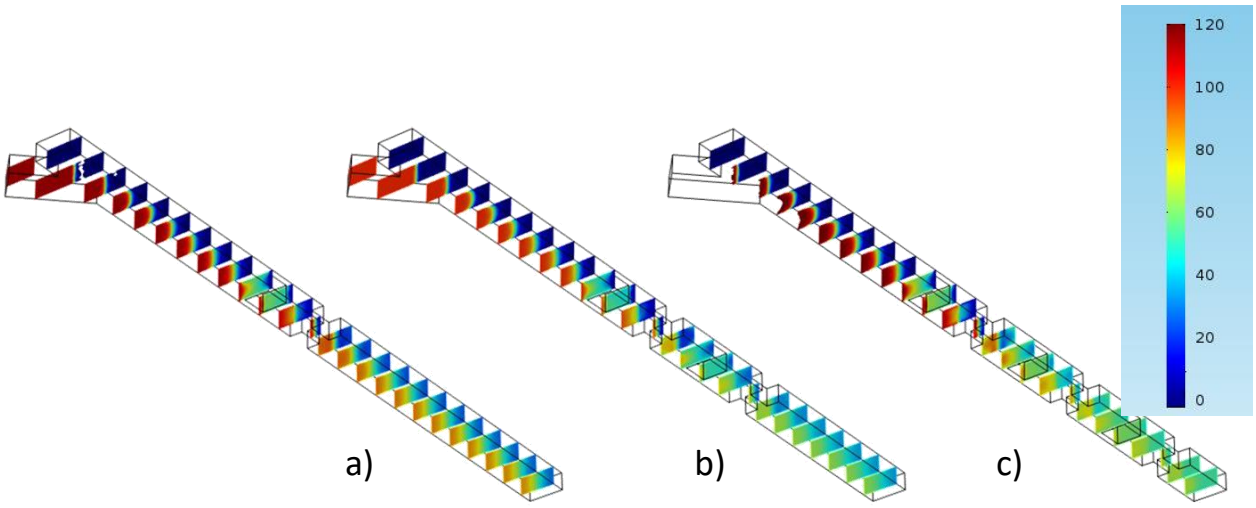

Figure 18 Concentration of the 0.7 mm square pillars (1-2) formation mesochannels, a) with 3 pillars, b) with 6 pillars and c) with 9 pillars. The mesochannels have 20 mm of length. Scale represents a colour code for the concentration gradient in mol/m^3. View of 25 XZ planes showing several cross-sections of the mesochannel

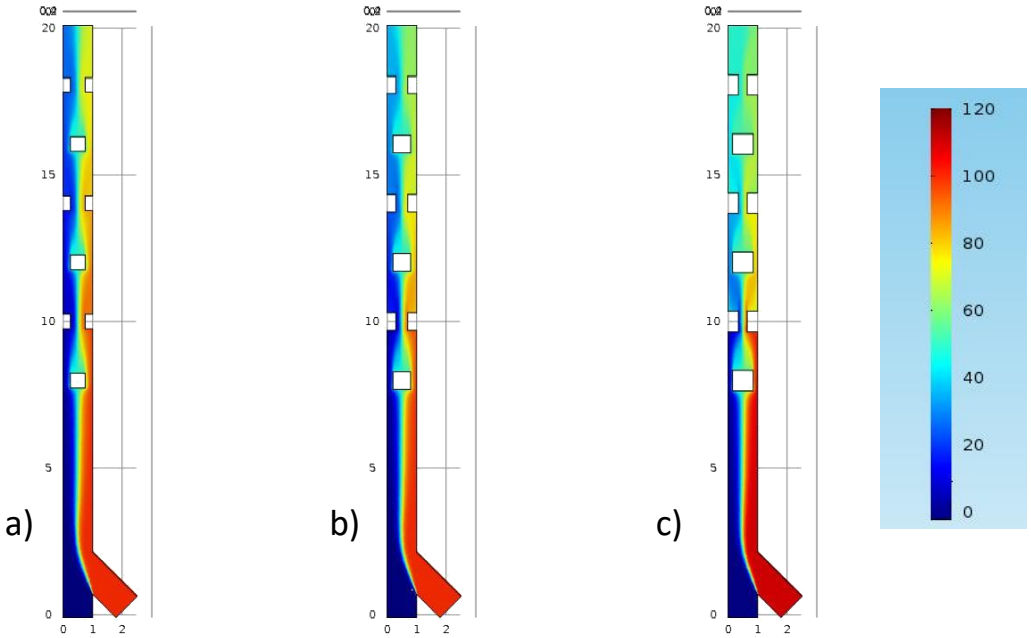

Figure 19: Concentration in square pillars (1-2) formation mesochannels with the following size of pillars: a)0.5mm side; b) 0.6mm side; and c) 0.7mm side. The mesochannels have 20 mm of length. Scale represents a colour code for the concentration gradient in mol/m^3. View of a XY plane crossing the middle of the mesochannel

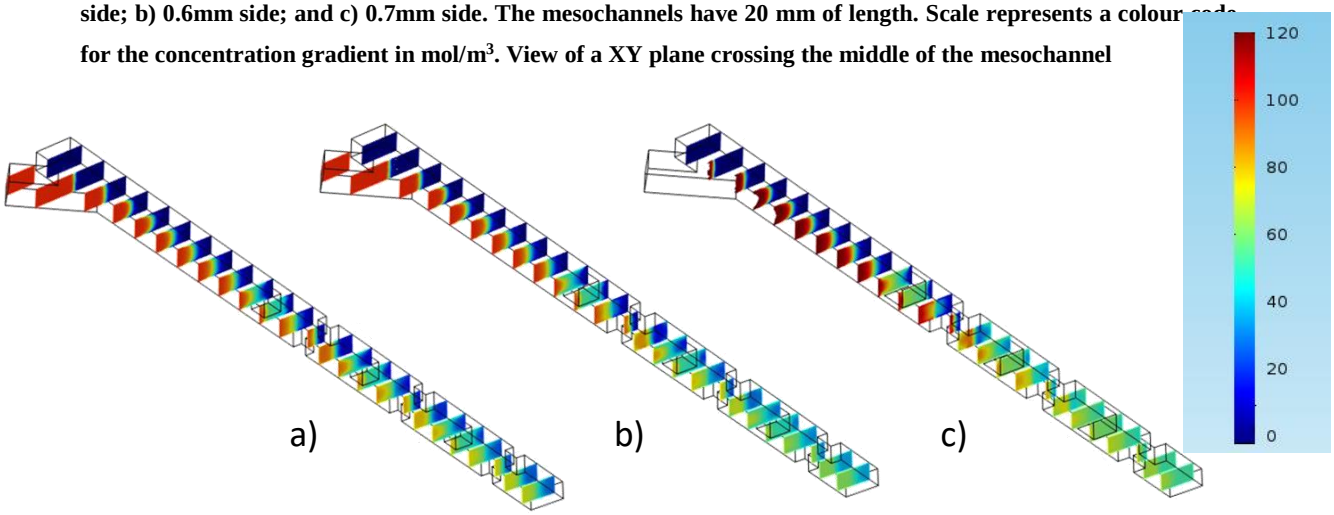

Figure 20 Concentration in square pillars (1-2) formation mesochannels with the following size of pillars: a)0.5mm side; b) 0.6mm side; and c) 0.7mm side. The mesochannels have 20 mm of length. Scale represents a colour code for the concentration gradient in mol/m^3. View of 25 XZ planes showing several cross-sections of the mesochannel

Alike the (1-1) square pillars formation mesochannels, mixing increases with greater size of the obstacles and with greater number of them, but also has the same challenges with changing the size of the pillars. Although, since (1-2) formation possesses more obstacles than the (1-1) formation, mixing is better on the former mesochannels as expected.

2.3.1.4 Simulation of Curved channels

Curved microchannel was chosen for their compactness in the design and to study the effect on mixing due to their non-uniform shapes.

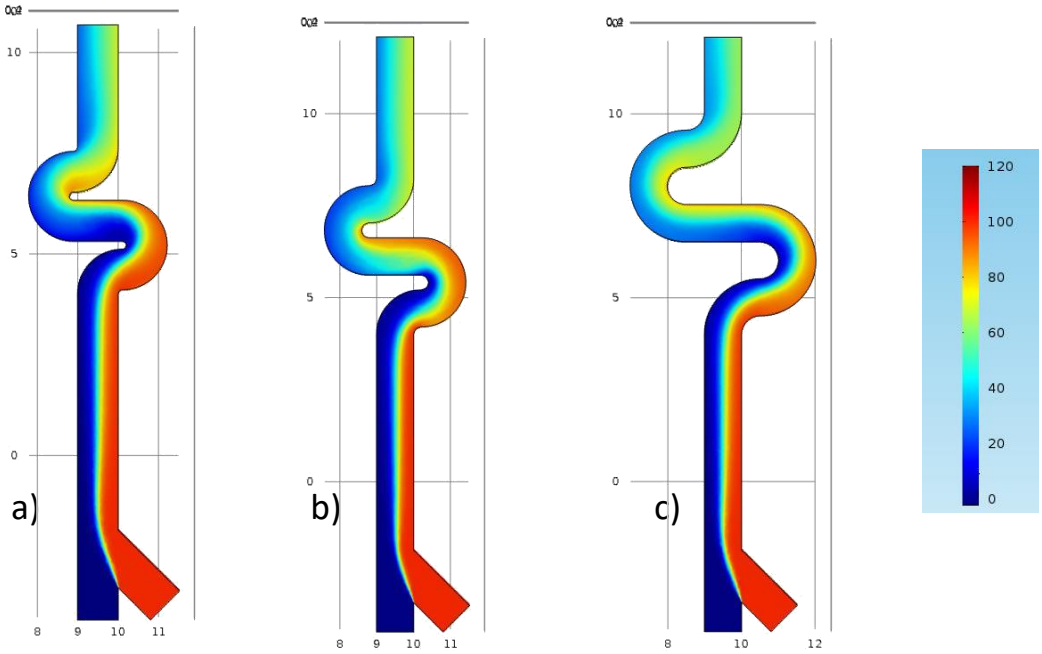

Figure 21: Concentration in curved mesochannels with different curve diamenter, as such the inner diamenter of the curves are: a)0.2mm; b) 0.4mm; and c) 1.0 mm. Scale represents a colour code for the concentration gradient in mol/m^3. View of a XY plane crossing the middle of the mesochannel

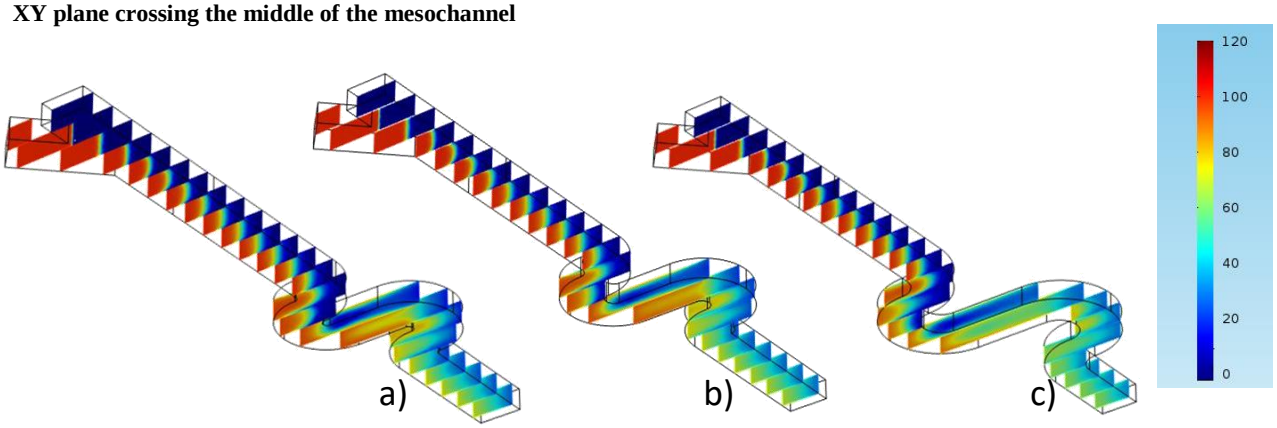

Figure 22 Concentration in curved mesochannels with different curve diamenter, as such the inner diamenter of the curves are: a)0.2mm side; b) 0.4mm side; and c) 1.0 mm side. Scale represents a colour code for the concentration gradient in mol/m^3. View of 25 XZ planes showing several cross-sections of the mesochannel

Simulations suggest that mixing is better with wider curves, however with narrower curves, despite having a slightly worst mixing, the length of the structure is significantly reduced. Since one of the objectives, is to make a structure as small as possible, the overall length of the structure will also have to be equated to optimize mixing with the shortest length possible.

2.3.1.5 Simulation of different inlet velocities in different inlets

This simulation was designed to test the effect of different inlet velocities would have on mixing, for that purpose three straight mesochannels were tested: one straight channel with the same inlet velocity; another with the inlet on the left with double the velocity of the right; and another channel with the double inlet velocity on the right than on the left.

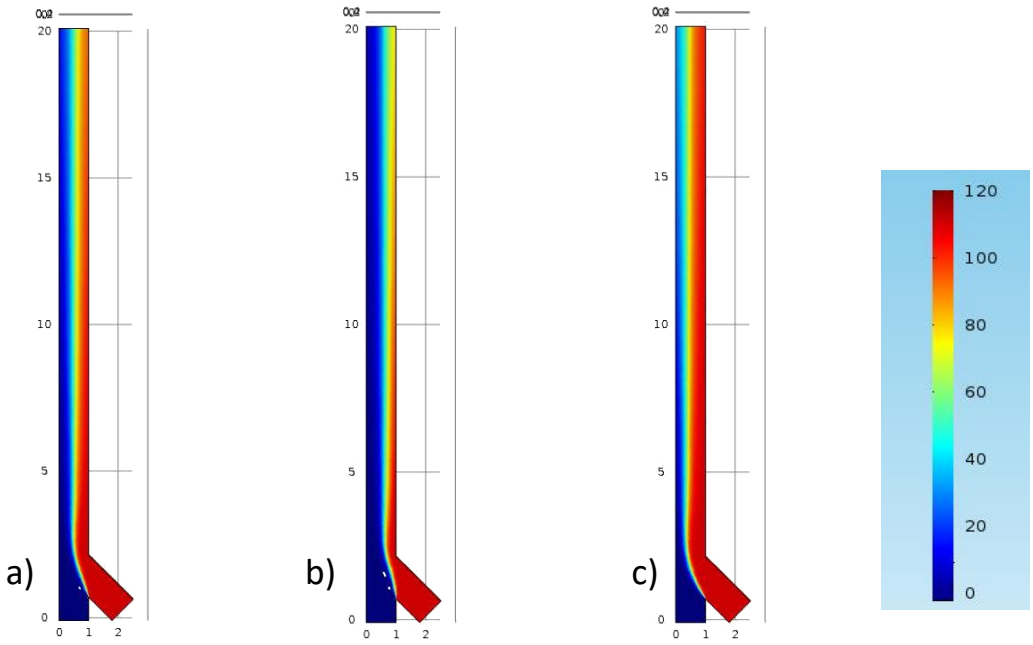

Figure 23: Concentration of the straight channels with 45ºangle between inlet, a) with both inlets with 0,042 m/s of inlet velocity; b) with 0.084 m/s of inlet velocity on the left inlet and 0.042 m/s on the right; and c) with 0.084 m/s of inlet velocity on the right inlet and 0.042 m/s on the left. The mesochannels have 20 mm of length. Scale colour code for the concentration gradient in mol/m^3. View of a XY plane crossing the middle of the mes

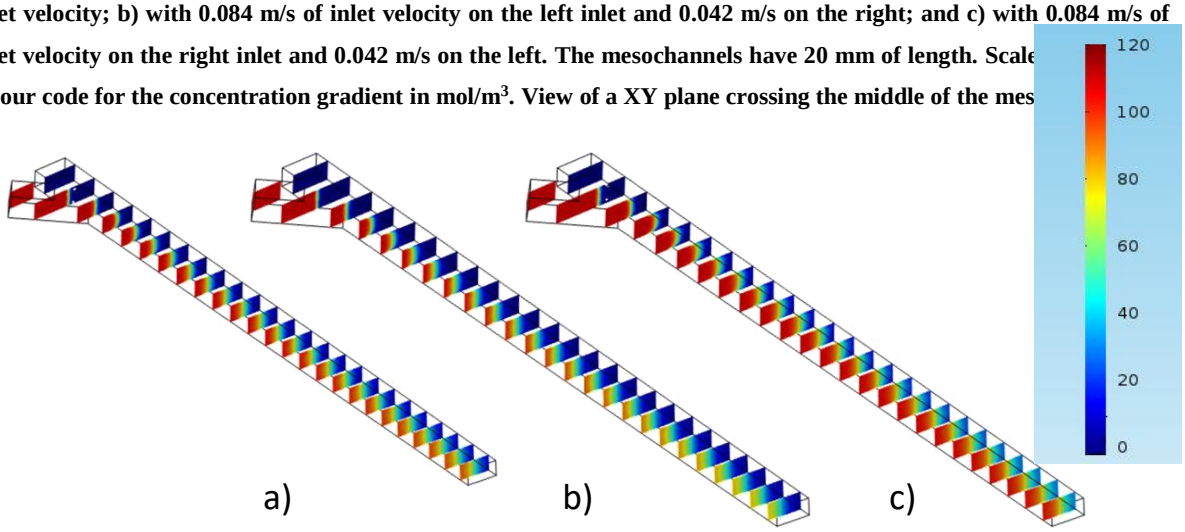

Figure 24 Concentration of the straight channels with 45ºangle between inlet, a) with both inlets with 0,042 m/s of inlet velocity; b) with 0.084 m/s of inlet velocity on the left inlet and 0.042 m/s on the right; and c) with 0.084 m/s of inlet velocity on the right inlet and 0.042 m/s on the left. The mesochannels have 20 mm of length. Scale represents a colour code for the concentration gradient in mol/m^3. View of 25 XZ planes showing several cross-sections of the mesochannel

As it can be seen, different velocities in different inlets do not produce any significant change in the mixing, which means that if the flowrate of two solutions are different it is safe to assume to have similar mixing requirements as if the flowrates were the same.

2.3.2 Simulation of Generation-1 Mesochannels

After experimental testing of Generation-0, it was noted that despite curved mesochannels were capable of being manufactured into working conditions, the channel was either too short or had too little flow disruption to produce any significant mixing. As such longer and more complex curved mesochannels were designed, simulated and then tested. So further simulations were carried out using different shapes for the curved mesochannels to determine the overall impact of the channels shape and different inlet velocities in the mixing.

The new mesochannels were designed using AutoCAD 2016, by replicating the same curve several times and arranging the resulting structure into: a short curved channel (ShM), a U-shaped curved channel (UM), a S-shaped curved channel (SM) and a longer curved channel (LM) (Figure 25).

These designs were later uploaded into COMSOL Multiphysics 5.0 in the geometry section and then converted into 3D models by extruding height of 0.5 mm, and simulations were carried out as described in the beginning of **Chapter 2.3**, with various inlet velocities, to determine if mixing can be achieved with slower velocities.

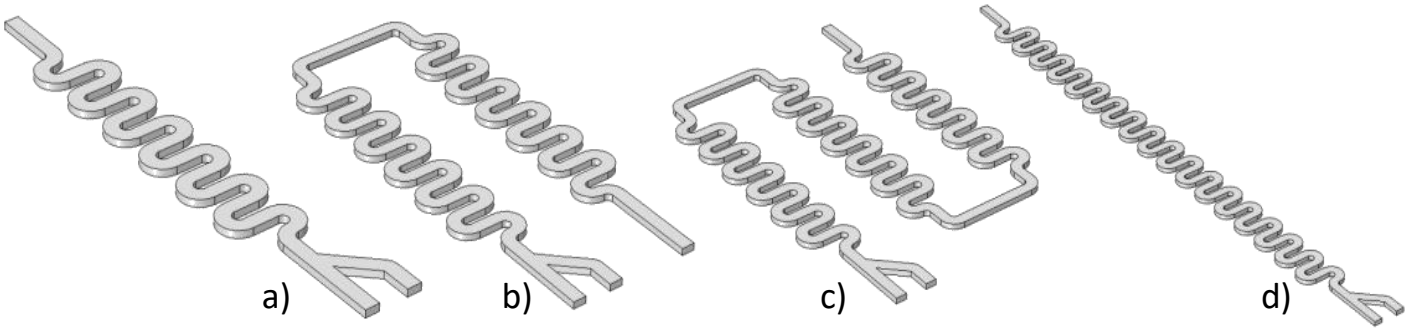

Figure 25: Models for the Generation-1 mesochannels: a) short curved mesochannel (ShM); b) U-shaped curved mesochannel (UM); c) S-shaped curved mesochannel (SM); d) long curved mesochannel (LM). Cross section in all mesochannels is 0.5 mm high and 1.0 mm wide

2.3.2.1 Simulation of Short Curved Mesochannels (ShM)

The Short Mesochannels (ShM) are the simplest design for stacked curved mesochannels, and as shown in figure below, complete mixing is estimated to happen somewhere between the fourth and the seventh U-turn, depending on the inlet velocity. If the experimental testing corroborates these simulations, or the full mixing onset occurs, for the specified inlet velocities, within the length of the ShM, there will be no need for more complex or longer channels.

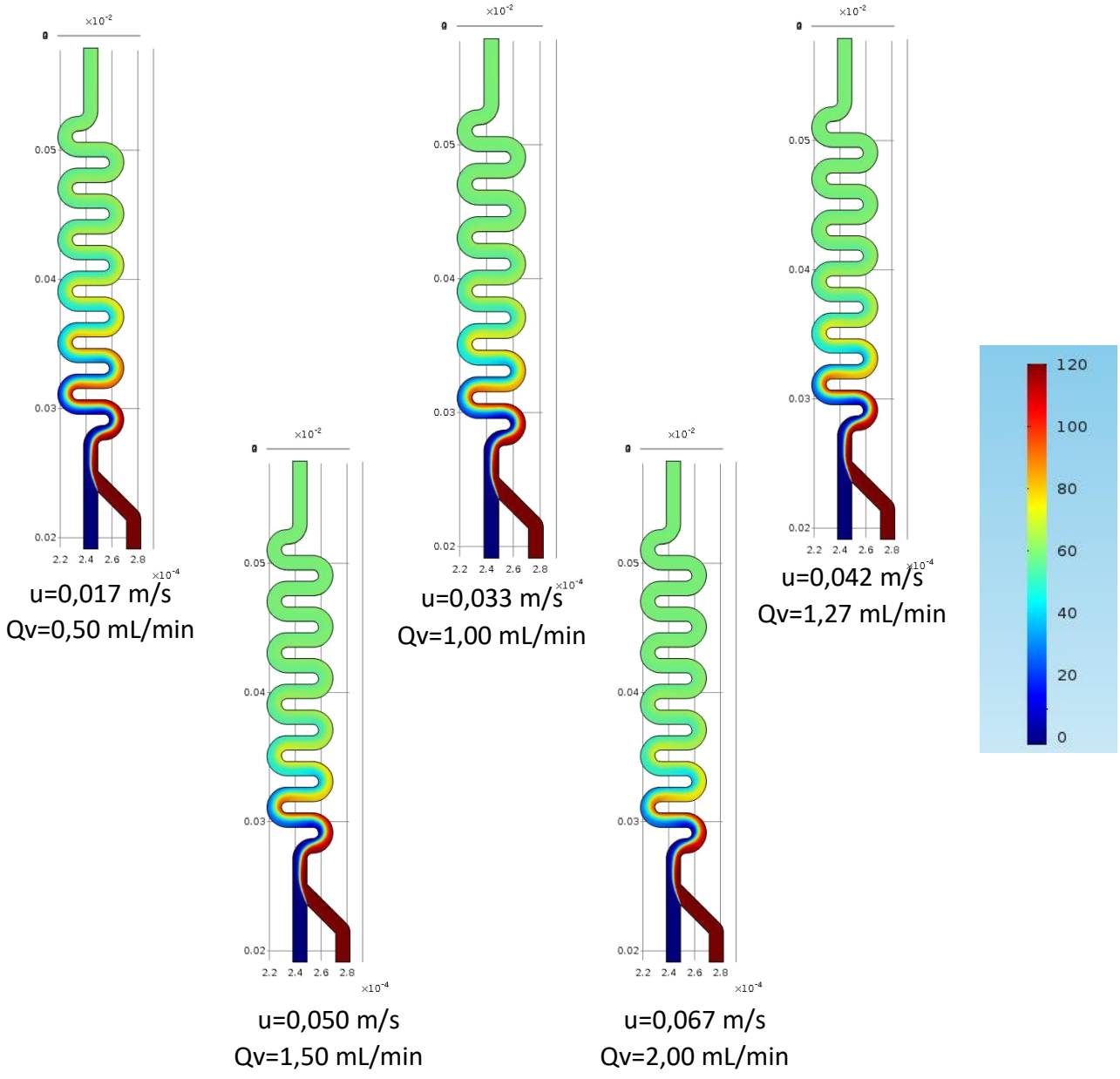

Figure 26: Simulations of Short mesochannels, with the inlet velocity on the bottom (same inlet velocity in both inlets). Dimension scale in meters. Scale represents a colour code for the concentration gradient in mol/m^3. View of a XY plane crossing the middle of the mesochannel.

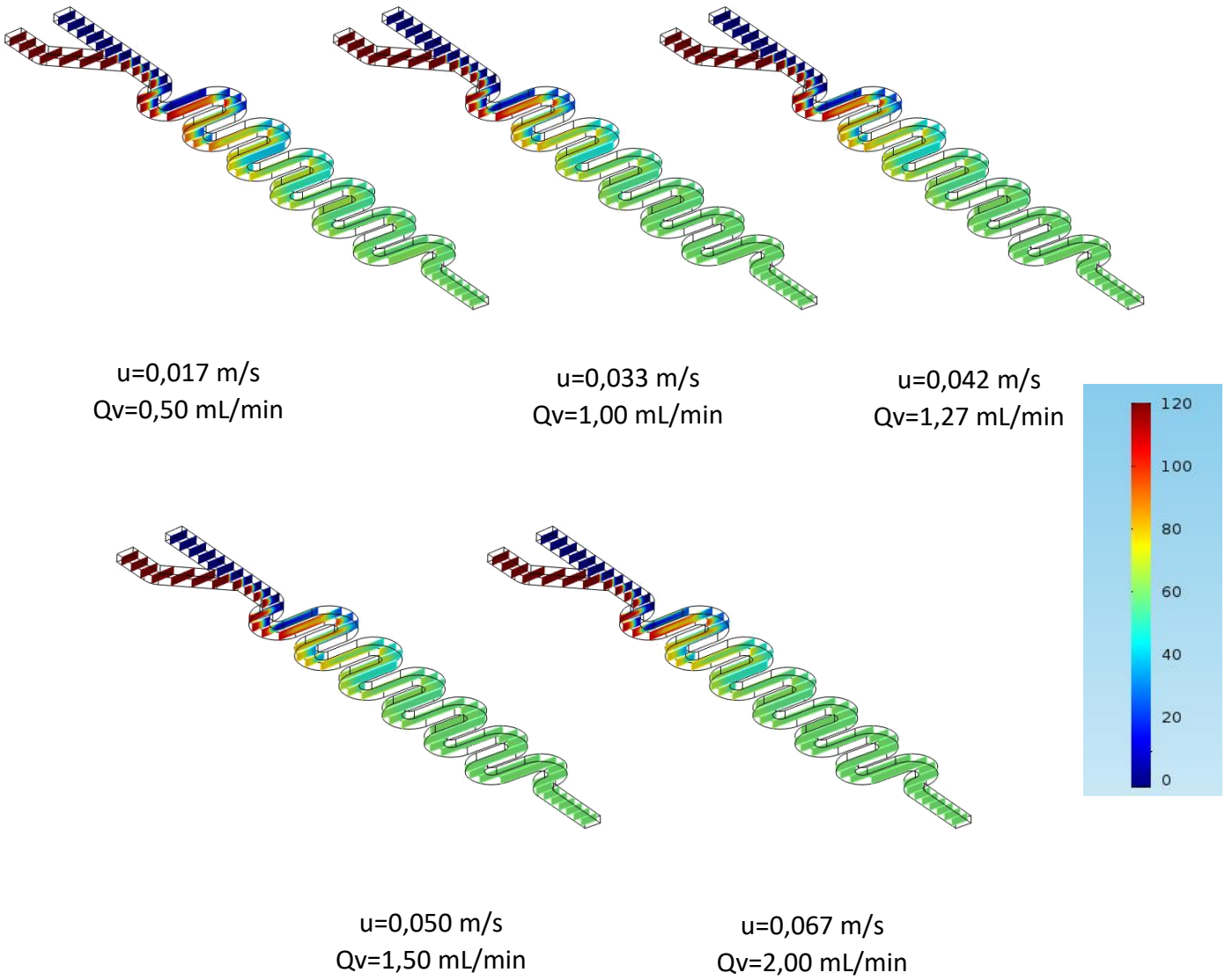

Figure 27 Simulations of Short mesochannels, with the inlet velocity on the bottom (same inlet velocity in both inlets). Dimension scale in meters. Scale represents a colour code for the concentration gradient in mol/m^3. View of 50 XZ planes showing several cross-sections of the mesochannel

2.3.2.2 Simulation of U-shaped Curved Mesochannels (UM)

U-shaped Curved Mesochannels (UM), were designed with two objectives in mind: to increase the length and complexity of the ShM, in the event, that the full mixing does not occur within the length of the ShM, also this design offers the possibility of arranging the inlets and outlets to be on the same side and close to each other, which translates in a simpler, smaller and closely packed structure for the entire chemical unit. As expected from the results observed in chapter 2.3.2.1, the same interval of to achieve full mixing is presented on the simulations of Figures 28 and 29, which means that full mixing is estimated to occur in between the fourth and the seventh U-turn.

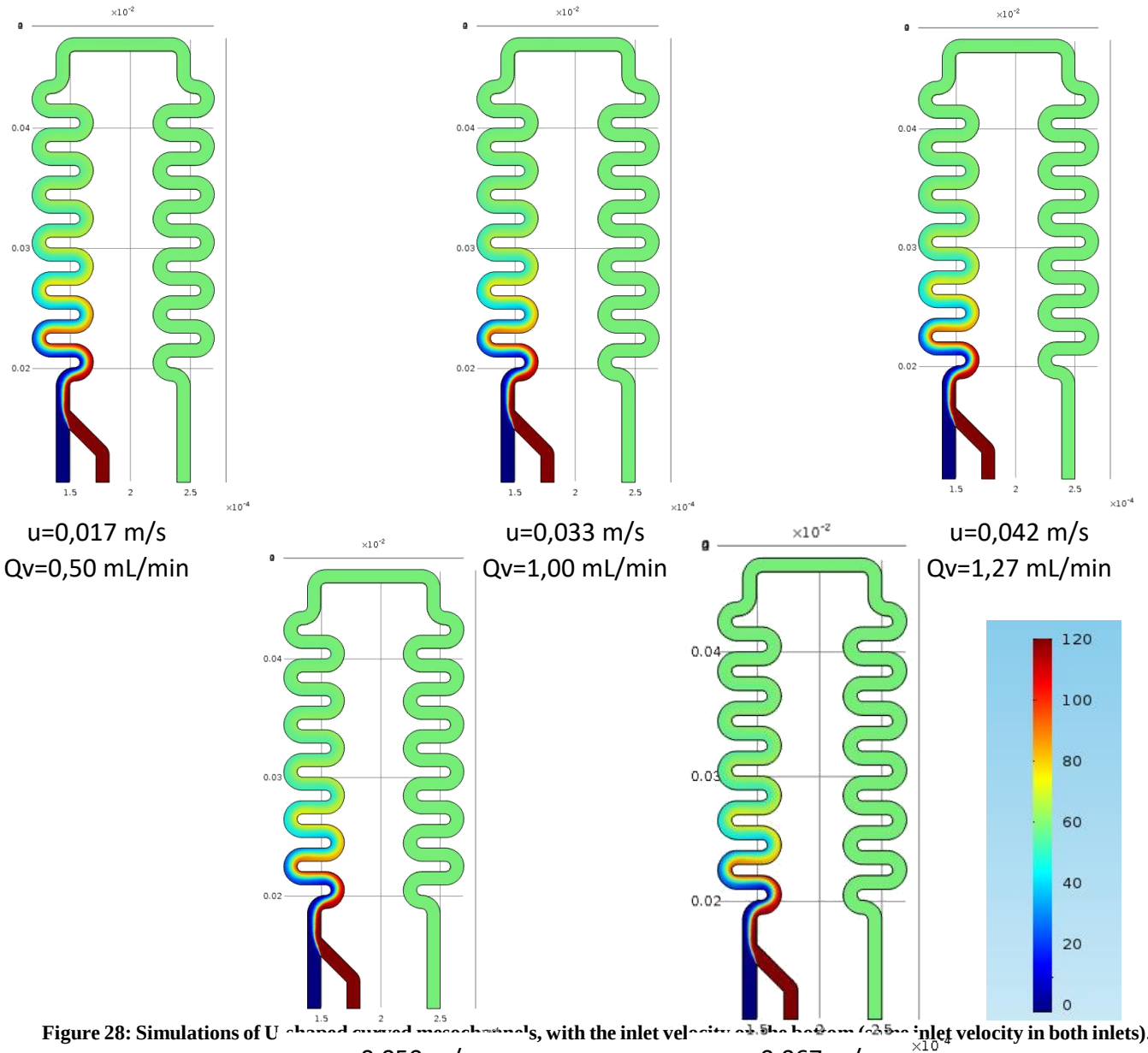

Figure 28: Simulations of U-shaped curved mesochannels, with the inlet velocity as the boundary condition (same inlet velocity in both inlets). Dimension scale in meters. Color scale for the concentration. View of a XY plane crossing the middle of the mesochannel.

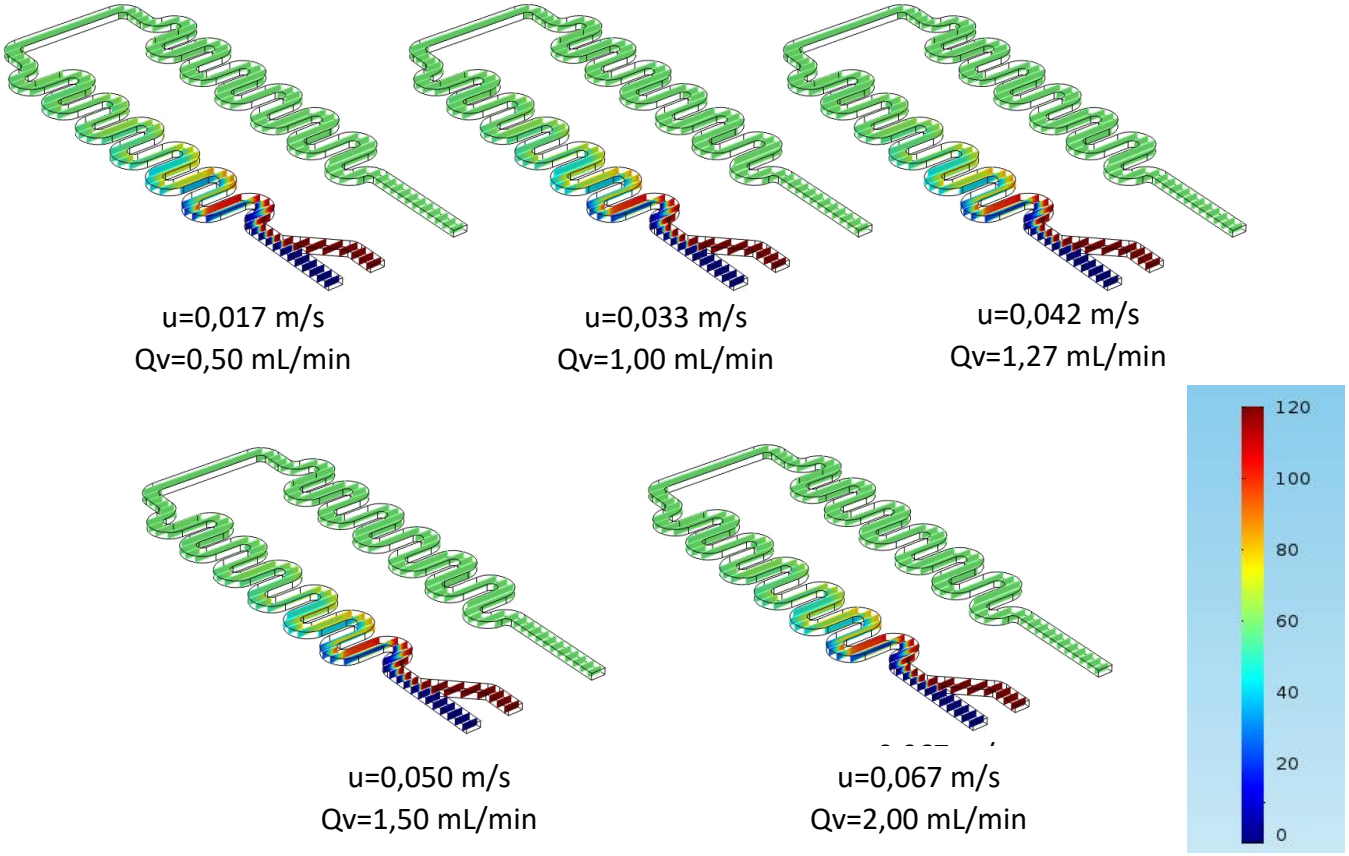

Figure 29 Simulations of U-shaped curved mesochannels, with the inlet velocity on the bottom (same inlet velocity in both inlets). Scale represents a colour code for the concentration gradient in mol/m^3. View of 50 XZ planes showing several cross-sections of the mesochannel

2.3.2.3 Simulation of S-shaped Curved Mesochannels (SM)

With even greater length and complexity than the UM, the S-shaped Curved Mesochannels (SM) were designed with the concern that mixing may not occur within the length of the previous mesochannels for the chosen inlet velocities. Alike the previous mesochannels, Figures 30 and 31, suggests that full mixing is estimated to occur somewhere between the fourth and the seventh U-turn.

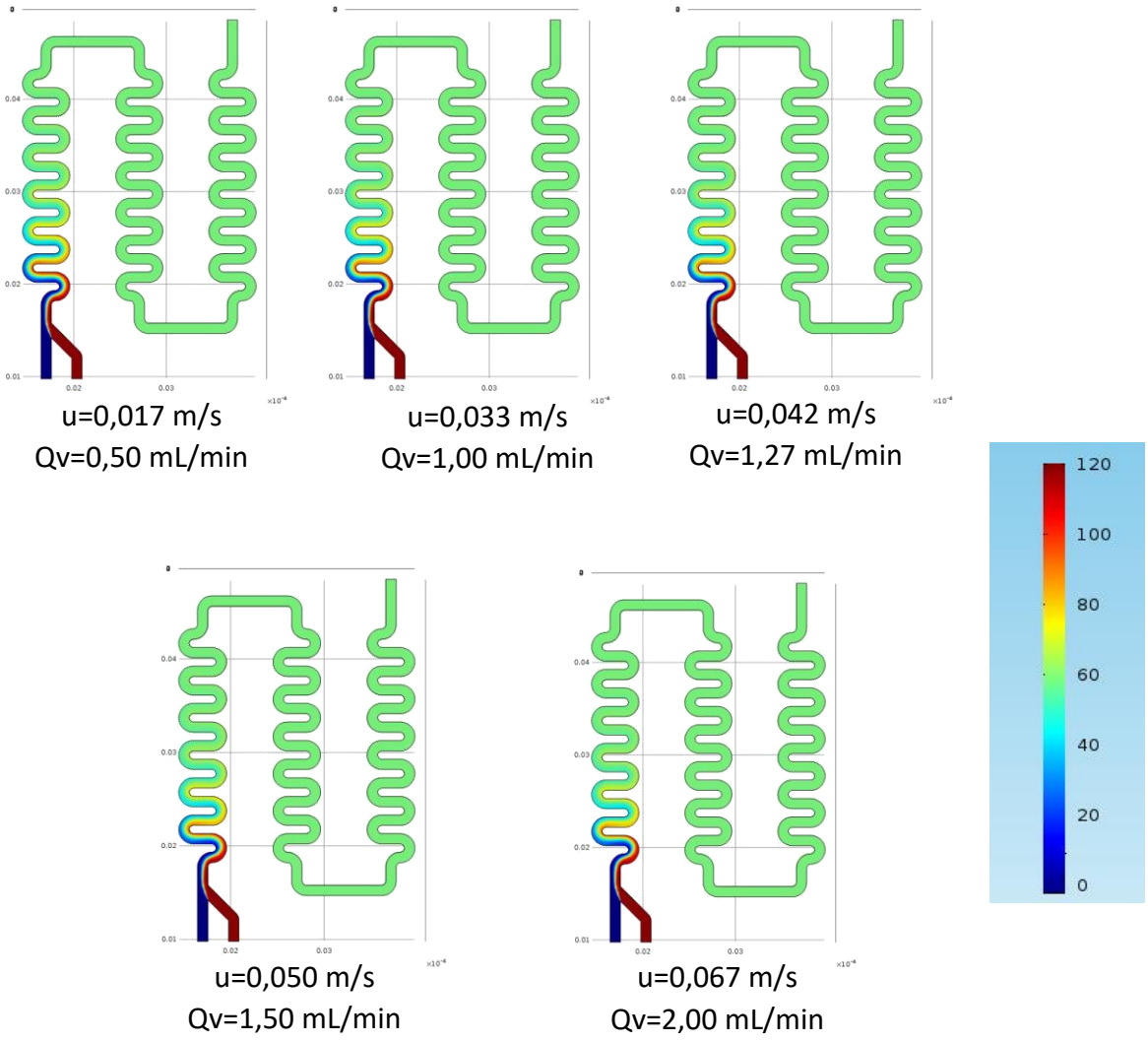

Figure 30: Simulations of S-shaped curved mesochannels, with the inlet velocity on the bottom (same inlet velocity in both inlets). Dimension scale in meters. Scale represents a colour code for the concentration gradient in mol/m^3. View of a XY plane crossing the middle of the mesochannel.

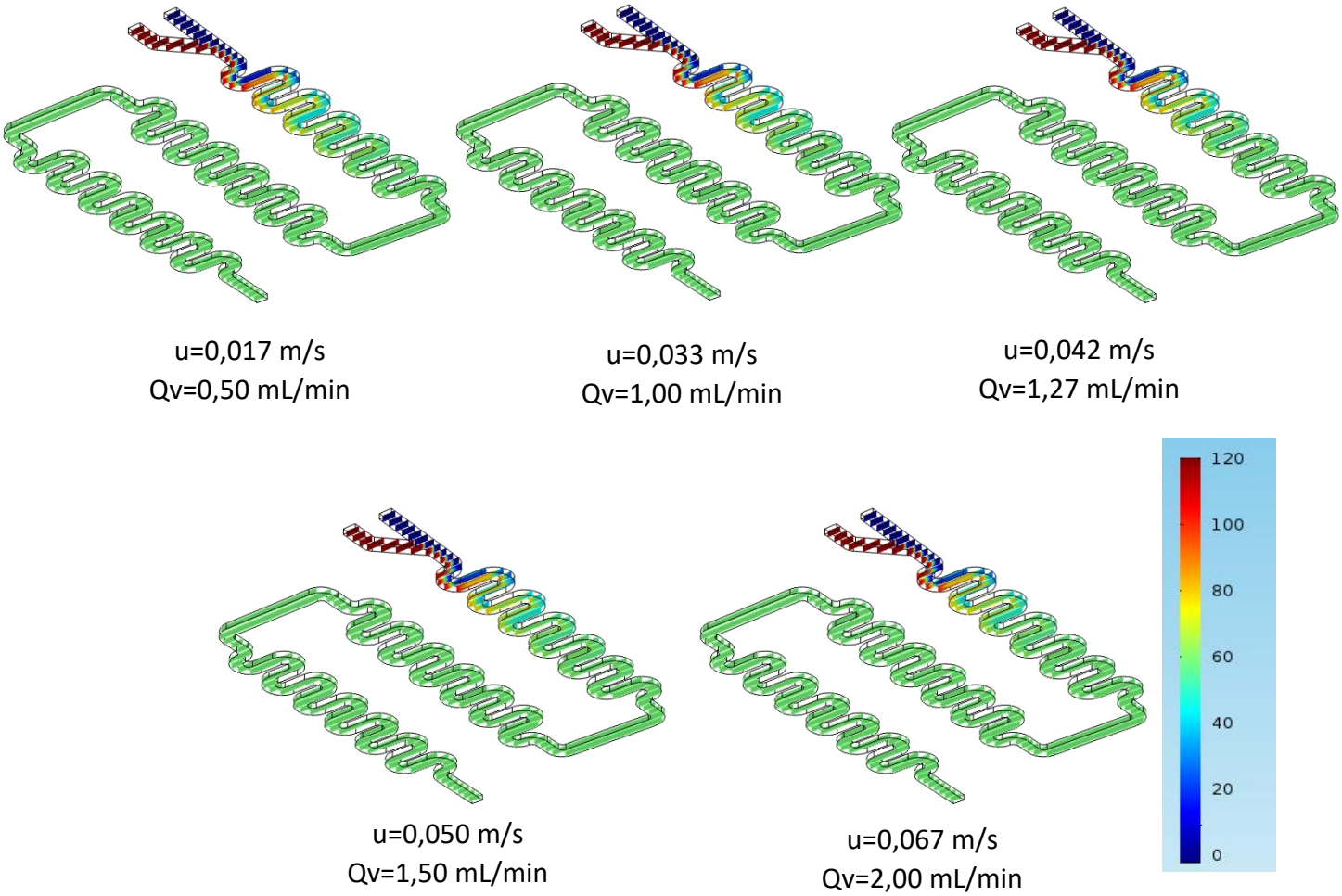

Figure 31 Simulations of S-shaped curved mesochannels, with the inlet velocity on the bottom (same inlet velocity in both inlets). Scale represents a colour code for the concentration gradient in mol/m^3. View of 50 XZ planes showing several cross-sections of the mesochannel

2.3.2.4 Simulation of Long Curved Mesochannels (LM)

Long Curved Mesochannels (LM) were designed out of the same concern behind the SM, and allows the possibility of determining the full mixing onset of a structure with a similar design as the ShM. Alike the previous mesochannels, Figures 32 and 33 suggest that full mixing is estimated to occur somewhere between the fourth and the seventh U-turn.

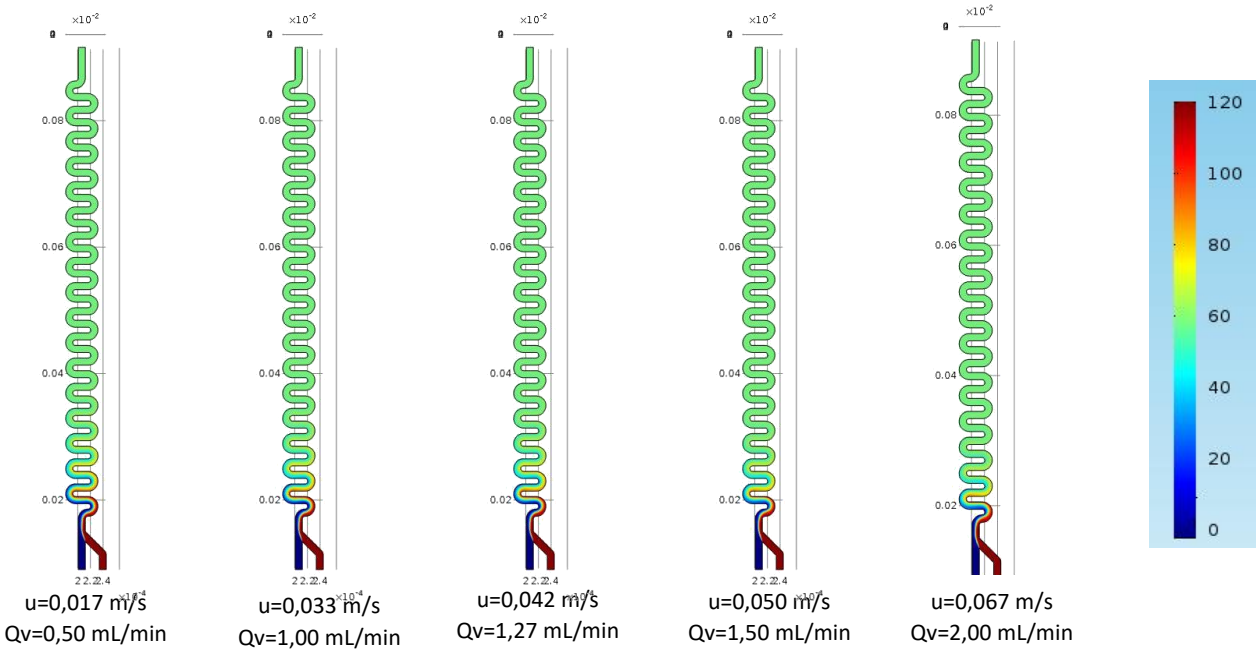

Figure 32: Simulations of Long curved mesochannels, with the inlet velocity on the bottom (same inlet velocity in both inlets). Dimension scale in meters. Scale represents a colour code for the concentration gradient in mol/m^3. View of a XY plane crossing the middle of the mesochannel.

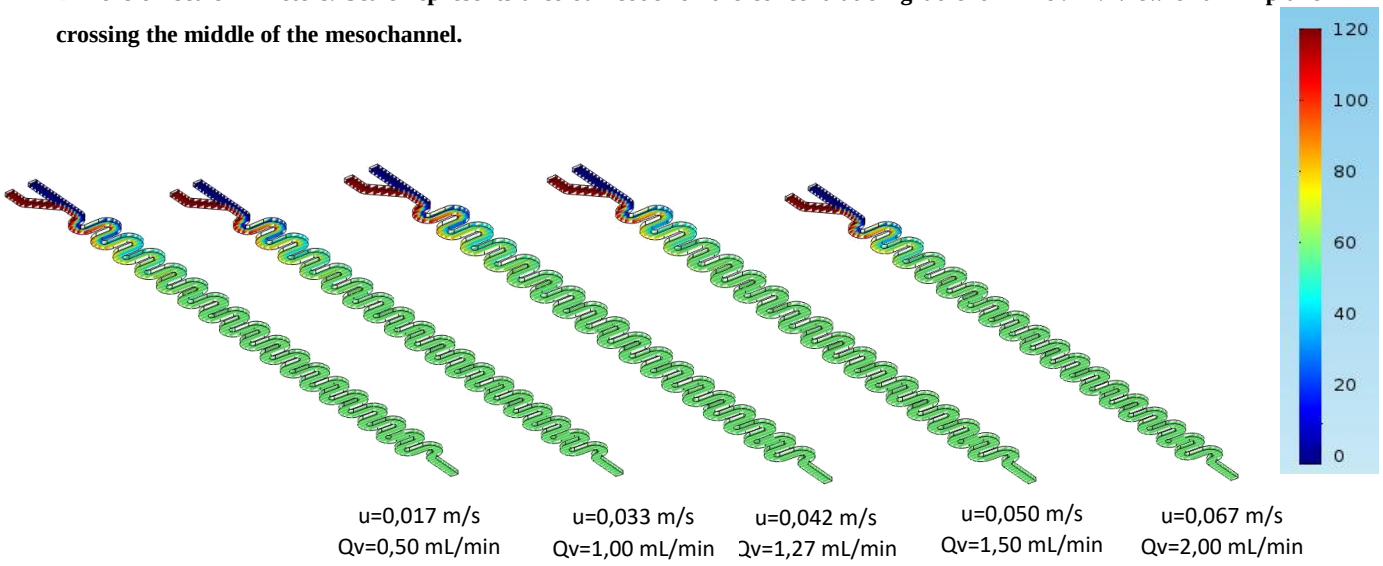

Figure 33: Simulations of Long curved mesochannels, with the inlet velocity on the bottom (same inlet velocity in both inlets). Scale represents a colour code for the concentration gradient in mol/m^3. View of 150 XZ planes showing several cross-sections of the mesochannel

3. Methodology

The methodology behind this thesis study of the miniaturization of the chemical unit of the SKALAR™ DOC analyser, begins by attempting to replicate mixing with smaller channels, since most of the process undergoing inside the chemical unit revolves around subjecting the sample to several reagents to convert inorganic impurities into CO_2 for immediate removal and converting organic matter into CO_2, these reactions will require an efficient mixing to achieve good conversion.

After simulation of several mesochannels with different designs, the ones showing the best mixing efficiency are selected for experimental testing. This testing involves creating structures of Poly (methyl 2-methylpropenoate), more commonly known as Poly(methyl methacrylate) (PMMA) or acrylic, of the selected mesochannels and pumping MilliQ water coloured with food dye into the aforementioned mesochannels.

To produce the PMMA structures, first the selected designs are converted into schematics using *AutoCAD 2016*, the selected designs of the structures was created with the white lines representing the mesochannels and the green lines representing the holes where the silicone tubbing is introduced, to make the inlets and outlets, and large red rectangles represent the areas designated for milling to remove 0.5 mm depth of PMMA around the samller red squares and rectangles to produce the square pillars.

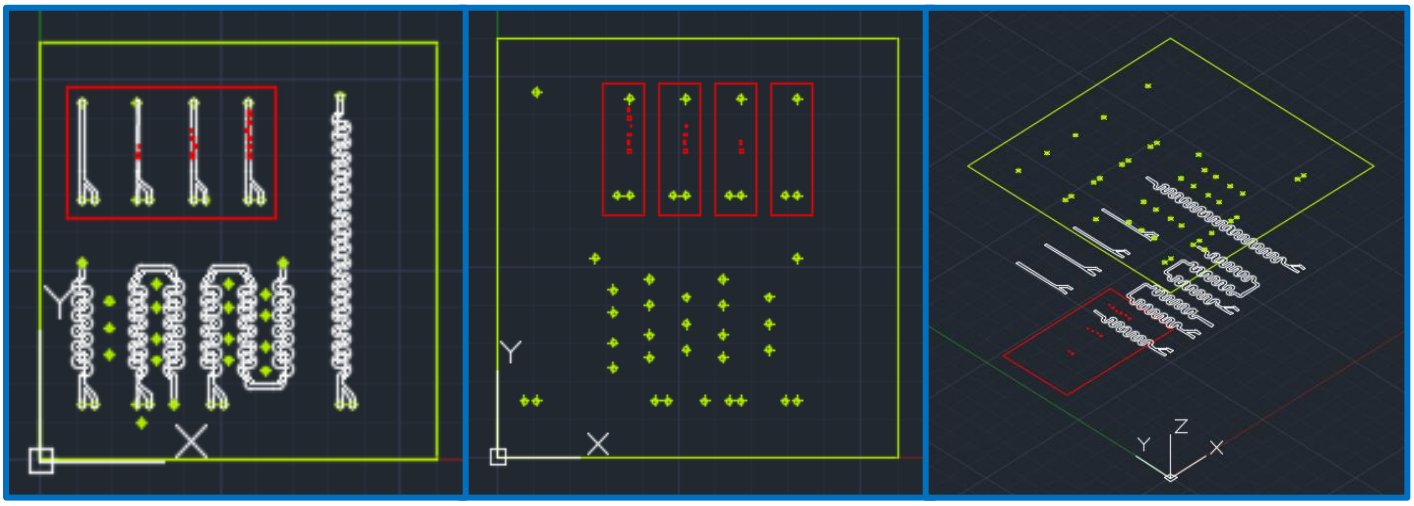

Figure 34: AutoCAD 2016 schematics for the PMMA structures, bottom piece on the left, top piece in the middle and isometric view of the the three layers separated into three different Z levels on the right. White represents the mesochannels, green the holes for silicone tubbing and in red the square pillars and areas to be milled.

These schematics are later milled using a 1.0 mm endmill and drilled with a 1.5 mm drill into a piece of PMMA using a Milling Machine, for that the toothpaths were created using a *DESKAM 2000*.

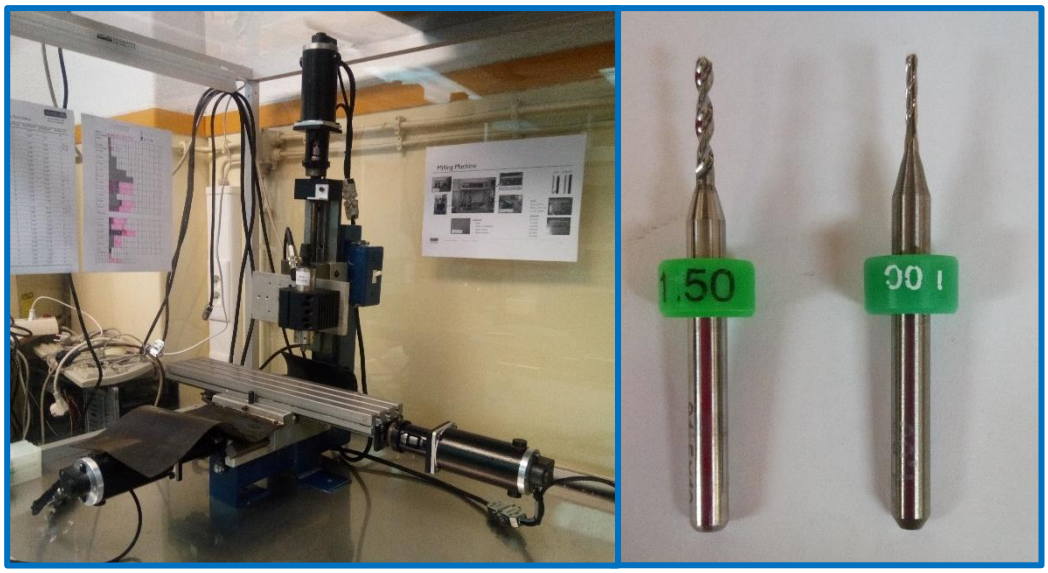

Figure 35 On the left, the Milling Machine employed to produce the mesochannles, On the right, the drill bit and mill bit employed in drilling and milling (1.5 mm and 1.0 mm respectively)

After milling and drilling both pieces of PMMA, they are fused together by solvation using acetone, for that purpose, it is required to drill a few extra holes for pouring acetone between the PMMA slabs, to cover the entire surface of both slabs and thus properly seal the mesochannels, avoiding leaks from one channel to another or the fluid taking "shortcuts" instead of following the desired path.

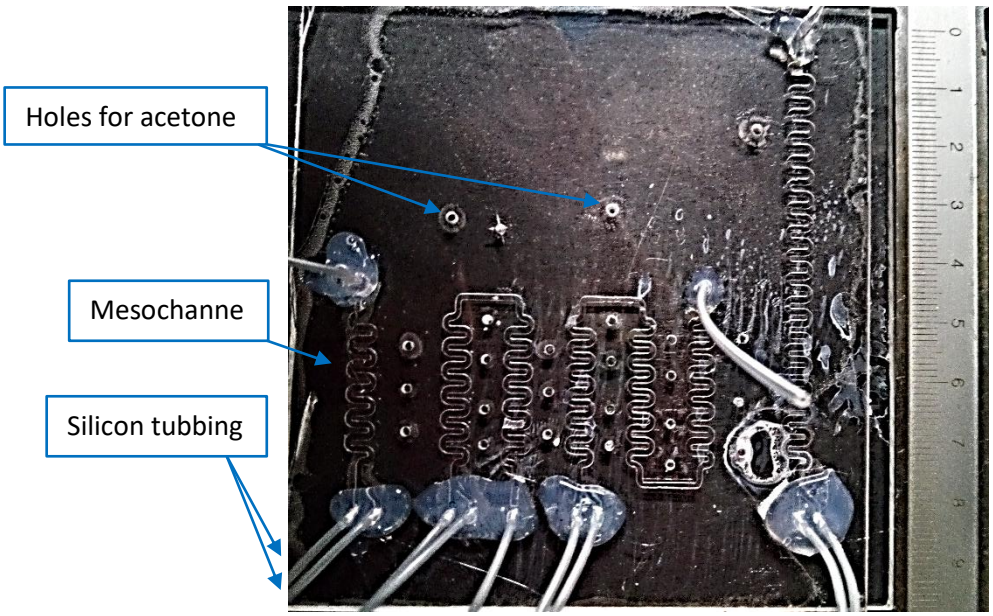

Figure 36: Top view of the PMMA structures used in the experimental tests, with silicone tubbing already attached to the proper holes in the PMMA. Calliper as reference on the left for scale.

3.1 Assembling Generation-0 Mesochannels

After analysis of the Generation-0 simulations, it was conclude that ,apart from the straight mesochannels, all mesochannels types showed a good degree of mixing, and for the experimental testing, the curved mesochannels and (1-1) square pillars formation were initially selected. The (1-2) formation channels, however, were not selected in the initial testing because they required a mill with a smaller diameter than the available at the time, so the (1-1) formation channels were manufactured first.

Nevertheless, the (1-1) formation channels presented several problems with manufacture, they would frequently be produced with obstructions that completely block any fluid flow. This happens because when the structures are fused together using acetone, and at several points of the mesochannel, channel is narrower to the point that the acetone contacts with the pillars and flows into the channel fusing the walls and the pillars together, blocking flow passage. The same issue also affects the (1-2) square pillars formation mesochannels, since they also have choke points, where the channel gets narrower, some points even narrower than the (1-1) square pillars formation mesochannels.

Thus, only the curved shaped design could proceed with further testing, since both (1-1) and (1-2) formation mesochannels could not be reproduced for testing with the available equipment.

It is important to mention that curved shaped mesochannels possess an advantage compared to the other types, they can be replicated in a closely packed fashion, meaning that in the likely event that it is necessary replicate the structure to obtain better mixing or longer residence time the resulting structure will not be as wide nor be as long as with the other mesochannels types.

3.2 Assembling Generation-1 Mesochannels

In the first attempt at manufacturing the Generation-1 mesochannels, the inner diameter of the curves was set at 0,4 mm, in an attempt to minimize the size of the mesochannel without compromising too much the mixing efficiency. During the milling, however, it was noticed that the mill often broke the curves because they were too thin, as such in the next designs the inner diameter was doubled, 0,8 mm, successfully preventing the mill from breaking the curves.

Another issue that occurred, was that, although, it is possible for curved mesochannels to be assembled into working conditions, despite numerous attempts, assembly of UM mesochannels in working conditions was never successful. The problem resides with the amount of acetone used to fuse the PMMA slabs, too much means that acetone flows into the channels, fusing them, and too little means that the mesochannel is not properly sealed and leaks occur. This problem affects all Generation-1 mesochannels, however after several attempts, it was possible to produce a working ShM, a SM and a LM, but unfortunately not an UM.

4. Experimental Testing

4.1 Setup for Mesofluidic Testing

4.1.1 Materials

1) silicone tubbing (OD=1.27 m; ID= 0.83 mm)
2) food colouring (red and blue)
3) 2 falcon tubes
4) PMMA structure
5) 2 syringe pumps
6) 3 syringes (10 mL)
7) 3 tubbing adapters
8) 3 syringe tips
9) Milli-Q water

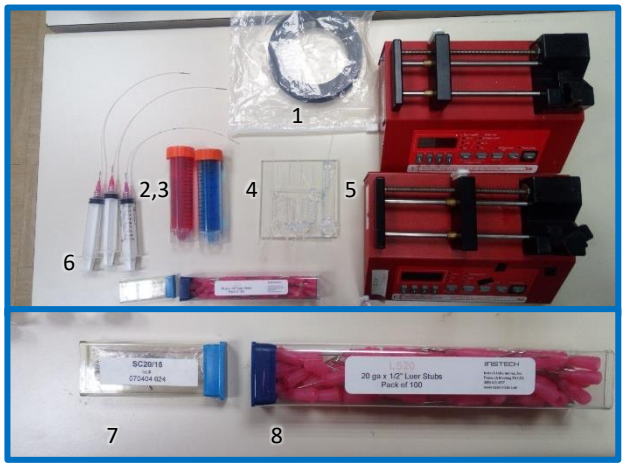

Figure 37 Materials employed in the experimental testing

4.1.2 Assembly

Firstly, the coloured solutions were prepared in two falcon tubes, one for red solution and the other for blue, by dissolving 20 drops of the respective dye with 50 mL of Milli-Q water. Then the syringes are filled with these solutions and placed on the syringe pump. Each syringe is assembled with a needle tip, attached to a roughly 15 cm long piece of silicon tubbing, which in turn connects to tubbing adapter. During the testing these syringes will be connected to the mesochannels inlets through the tubbing adapter.

For the outlets, the similar construct is assembled: a syringe with a needle tip attached to a silicon tubbing which is in turn attached to a tubbing adapter that will connect with the mesochannel outlet. However, for the outlets, there is no need for a syringe pump and the plunger is removed, the single purpose of the third syringe is to act as a recipient for the coloured fluid leaving the mesochannel through the outlet. The adapters are then disconnected from the inlets and outlet of one mesochannel to the other after all velocity tests have been carried out.

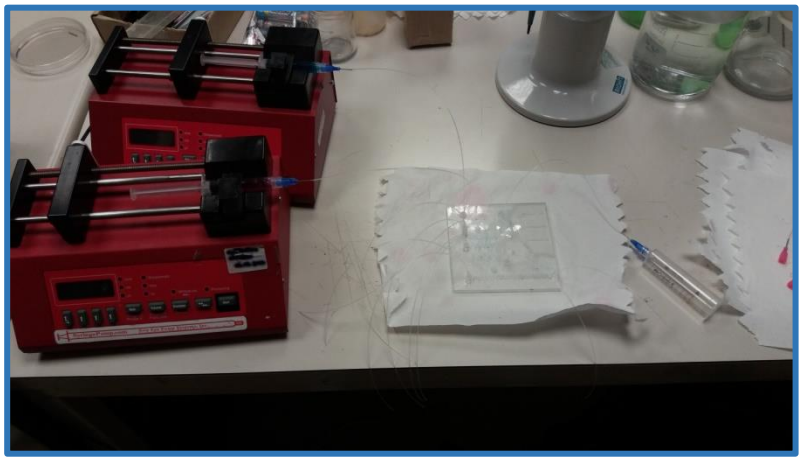

Figure 38: Setup assembled for experimental testing

4.2 Results and Discussion

The scope of these tests is to ascertain if mixing can be achieved in these mesochannels and test the effect of inlet velocity on the mixing. For that different flowrates were tested: 0.5 mL/min, 1.0 mL/min, 1.27 mL/min, 1.5mL/min and 2.0 mL/min.

Flow rate, Q (mL/min)	***0.50***	***1.00***	***1.27***	***1.50***	***2.00***
Reynolds number, Re	15.86	22.15	28.20	47.58	63.45
Hydraulic Diameter, D_H (m)	6.67×10^{-4}	6.67×10^{-4}	6.67×10^{-4}	6.67×10^{-4}	6.67×10^{-4}
Cross section area of the tube (m^2)	5.00×10^{-7}	5.00×10^{-7}	5.00×10^{-7}	5.00×10^{-7}	5.00×10^{-7}
Inlet velocity, u (m/s)	1.67×10^{-2}	3.33×10^{-2}	4.24×10^{-2}	5.00×10^{-2}	6.67×10^{-2}
Dynamic viscosity at 20ºC, μ (Pa.s)	1.00×10^{-3}	1.00×10^{-3}	1.00×10^{-3}	1.00×10^{-3}	1.00×10^{-3}
Volumetric Mass Density at 20ºC, ρ (Kg/m^3)	998.21	998.21	998.21	998.21	998.21

Table 4: Flow properties of various flowrates in the mesochannels

Unfortunately, when assembling the PMMA structures often excess acetone poured into the mesochannels, fusing them shut, which left them in non-working condition. And despite several tries in assembling the PMMA structure correctly, the U-shaped mesochannel was never operational and could not be tested with, however data collected from the other mesochannels, make up for this mishap.

Nonetheless, after analysis of the photos taken [Attachments B, C and D]and analysis using ImageJ program through the analyse option “RGB profile”, which decomposes the colour of the pixels from a pre-selected line into three colours, Red, Blue and Green, and measures their intensity. The criteria used to determine mixing is by measuring the colour intensity in the cross-section of the mesochannel, if the blue and the red lines do not change positions relatively to each other, then mixing is achieved, as it is shown in Figure 39. Then the number of U-turns before full mixing are counted and recorded on Table 5, in this thesis, U-turns are considered all curves that turn the direction of the flow by 180 degrees, as exemplified in Figure 39, in other words, U-shaped curves.

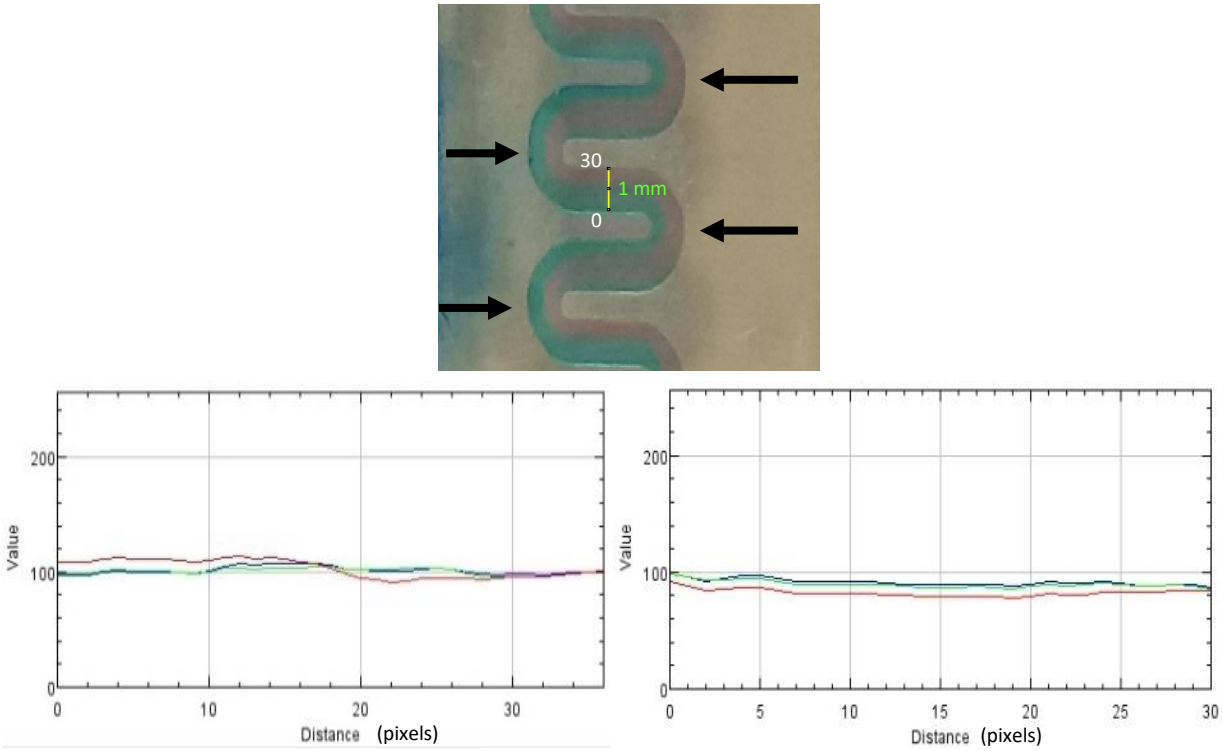

Figure 39: On the top, a representation of a cross section selected for analysis in ImageJ, also the 5 black arrows represent U-turn counting. On the bottom left, an RGB profile of a cross section, with the red showing a greater intensity in the first half of the cross section, and greater intensity of blueon the second half, suggesting incomplete mixing. On the bottom right, colour intensity seems uniform without alternating the colour of greater intensity, suggesting complete mixing. In the graphs, "Distance" is measured in pixels, and "Value" represents colour intensity which is a dimensionless measure.

Flow rates (mL/min)	*SM (36 turns)*	*LM (34 turns)*
0,50	N.M	N.M
1,00	N.M	N.M
1,27	36	N.M
1,50	35	N.M
2,00	31	34
3,00	24	26
4,00	23	24
5,00	22	21

Table 5: Number of U turns required to achieve full mixing in each channel. No mixing is represented by N.M.

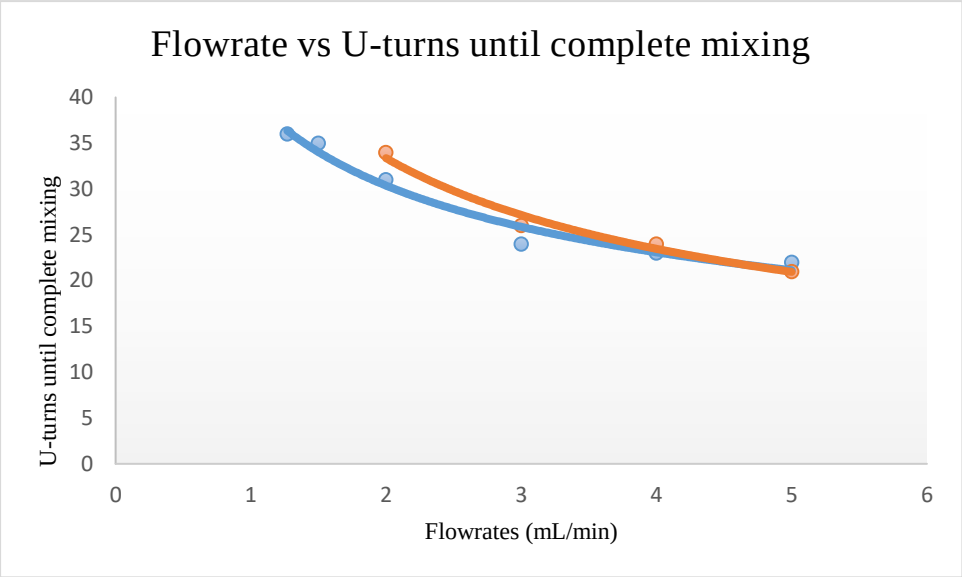

Figure 40 Representation of the full mixing onset on the SMs (in blue) and the LMs (in red) in a graph of Flowrate (mL/min) vs U-turns until complete mixing

During testing, as opposed to what the simulations suggested, ShM never showed full mixing, suggesting they required an even higher inlet velocity. As for the remainder working mesochannels, as it is shown in Table 3 and Figure 8, contrary to the simulation results for the flowrates from 0,5 mL/min to 2,00 mL/min, mixing did not occur between the 4th and 7th U-turn, where, in fact, only occurs on the longest mesochannels (SM and LM) with a minimum of 31 U-turns, and even then, the designed mesochannels were not long enough to achieve mixing with all the simulated flowrates. Because of this, there was not enough data to draw any valid conclusion, so, more tests were carried out with higher flowrates: 3.00 mL/min; 4.00 mL/min; and 5.00 mL/min.

With the results from extra inlet velocities, it can be concluded from the results that, with greater inlet velocities, mixing occurs earlier in the same structure, which means that the greater the velocity, the greater the mixing and shorter is the required structure.

5. Conclusion

From the obtained simulations and tests, one can see that mixing can be achieved in the proposed mesochannels, however there is a big discrepancy between the inlet velocities at which full mixing occurs. Determining the required length necessary for full mixing to occur is an important requirement to conjugate the length of the mesochannel with inlet velocity to optimize residence time.

This residence time is a key parameter to consider in building these mesochannels, since several reactions take place throughout the process and in the dialyser section, the diffusion of CO_2 through the Teflon membrane requires time. Having that in mind, this study suggests that it is possible to produce a closely packed mesochannel where both inlet velocity and size of the mesochannel can be adjusted to achieve full mixing with a specific residence time, without either creating a mesochannel too long or using too low of inlet velocities. To further test this hypothesis, this project would require more time and more complex PMMA structures, which are proving quite difficult to obtain since the Milling Machine is currently out of order.

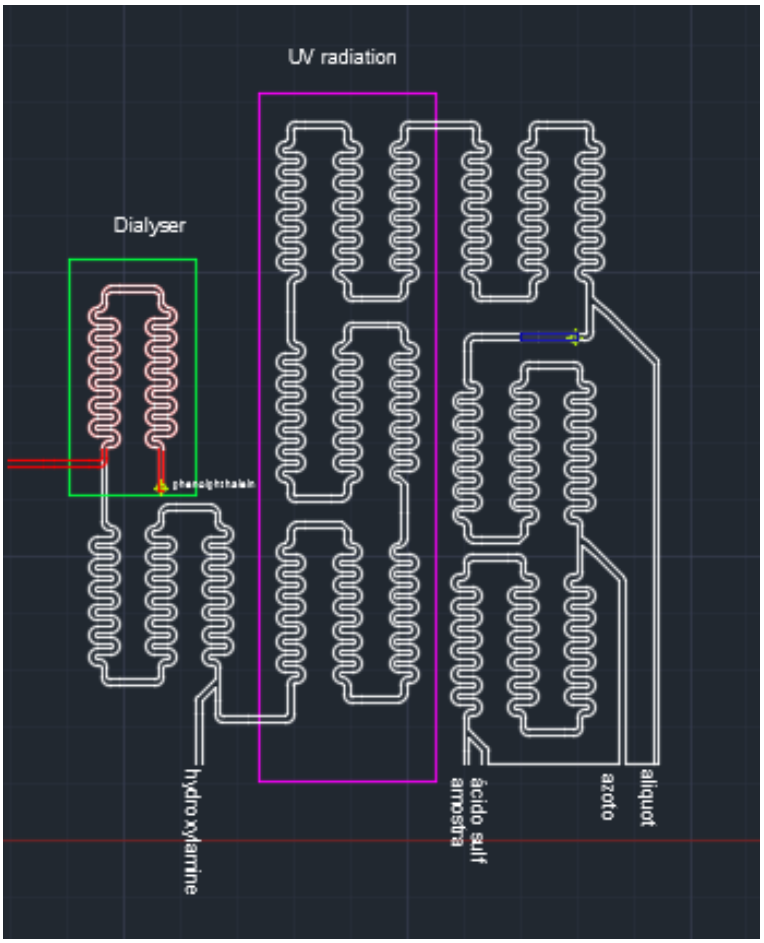

Figure 41 Mock schematics of the chemical unit. In white the mesochannels; in blue a small chamber with added height to separate the gaseous phase from the liquid, the purple rectangle represents the area allocated for UV radiation, the green rectangle represents the Teflon membrane in the dialyser, in yellow are portrayed the holes for outlets and inlets; and lastly in red represents a mesochannel that overlaps the white mesochannel in the dialyser, these mesochannels will be separated by the Teflon membrane. Dimensions: 11.83 cm x 11.51 cm

On a side note, results also show that the S-shaped mesochannel provides better mixing, since it possesses the lowest full mixing onset, in addition, it is the only mesochannel among the designed that allows mixing with the same flow regime as the original analyser (flowrate 1.27 mL/min).

Although, development of this analyser as yet to reach the testing stage of proof of concept, thus a lot of variants are yet to be tuned to optimize the device, the figure below shows a mock schematic for the chemical unit in AutoCAD 2016, which represents the first mesochannel for the chemical unit to be tested in the proof of concept stage, once it is possible to reproduce it in a PMMA.

In summary, this thesis set out to create a smaller device for analysing DOC, but due to the time limitation given to this project, the thesis could only cover the study of mixing and fluid dynamics inside the mesochannels. However given the outcome presented in the results, it can be concluded is possible to reduce the size of the chemical unit, using the S-shaped curved mesochannel, which showed the best mixing efficiency, and adjusting both inlet velocity and length of mesochannels. These adjustments will be performed in greater depth on the "proof of concept" stage, which preparations are currently underway.

6. Bibliography

1. Monica Z. Bruckner, Montana State University B. Measuring Dissolved and Particulate Organic Carbon (DOC and POC) [Internet]. Available from: http://serc.carleton.edu/microbelife/research_methods/biogeochemical/organic_carbon.html

2. Saskatchewan G. Dissolved Organic Carbon (DOC) [Internet]. Government of Saskatchewan. 2009 [cited 2016 Oct 25]. Available from: http://www.saskh2o.ca/PDF-WaterCommittee/DissolvedOrganicCarbon.pdf

3. Aiken GR, Mcknight IDM, Thorn IKA, Thurman EM. Isolation of hydrophilic organic acids from water using nonionic macroporous resins Hydrophobic acids XAD - 4 ~ I NaOH). Hydrophilic acids. Org Geochem. 1992;18(4):567–73.

4. Aiken G, Cotsaris E. Soil and hydrology: Their effect on NOM. J / Am Water Work Assoc. 1995;87(1):36–45.

5. Giancoli Barreto SR, Nozaki J, Barreto WJ. Origin of Dissolved Organic Carbon Studied by UV-vis Spectroscopy. Acta Hydrochim Hydrobiol. 2003;31:513–8.

6. Benner,R.; Von Bodungen, B.; Farrington, J.; Hedges, J.I.; Lee, C.; Mantoura, F.; Suzuki, Y.; Williams, P.M. Measurement of dissolved organic carbon and nitrogen in natural waters: Workshop report. Mar Chem. 1993;41(1–3):5–10.

7. Determination of dissolved organic carbon and total dissolved nitrogen in sea water [Internet]. 2007. p. 7. Available from: http://www.jodc.go.jp/geotraces/docs/PICESReport34_DOC_DON.pdf

8. Rene P. Schwarzenbach, Philip M. Gschwend DMI. Environmental organic chemist. Second edi. Wiley-Interscience a John Wiley &Sons, INC., Publication. 2003;

9. Weishaar J, Aiken G, Bergamaschi B, Fram M, Fujii R, Mopper K. Evaluation of specific ultra-violet absorbance as an indicator of the chemical content of dissolved organic carbon. Environ Sci Technol. 2003;37(20):4702–8.

10. Miller WL, Zepp RG, Obernosterer I, Benner R, Keiber JR, Zhou X, et al. Formation of carbonyl compounds from UV-induced photodegradation of humic compounds in the sea. Limnol Oceanogr. 1990;35(7):1503–15.

11. Boehm PD, Quinn JG. Solubilization of hydrocarbons by the dissolved organic matter in sea water. Geochim Cosmochim Acta. 1973;37(11):2459–77.

12. Krom MD, Sholkovitz ER. Nature and Reactions of Dissolved Organic-Matter in Interstitial Waters of Marine-Sediments. Geochim Cosmochim Acta. 1977;41(11):1565–73.

13. Deflandre B, Gagné JP. Estimation of dissolved organic carbon (DOC) concentrations in nanoliter

samples using UV spectroscopy. Water Res. 2001;35(13):3057–62.

14. Servais P, A. Anzil, Ventresque C. Simple method for determination of biodegradable dissolved organic carbon in water. Appl Environ Microbiol. 1989;55(10)(10):2732–4.

15. Brandstetter A, Sletten R. Estimating dissolved organic carbon in natural waters by UV absorbance (254 nm). Zeitschrift für, 1996;159:605–7.

16. Oliver BG, Thurman EM, Malcolm RL. The contribution of humic substances to the acidity of colored natural waters. Geochim Cosmochim Acta. 1983;47(11):2031–5.

17. Berggren D. Speciation and mobilization of aluminium and cadmium in podzols and cambisols of S. Sweden. 1992;125–56.

18. Hedges JI. Global Biogeochemical Cycles - Progress and Problems. Mar Chem. 1992;39(1–3):67–93.

19. Romankevich E a., Ljutsarev SV. Dissolved organic carbon in the ocean. Mar Chem. 1990;30:161–78.

20. Watanabe K, Badr E-SE-S, Pan X, Achterberg EPEP. Conversion efficiency of the high-temperature combustion technique for dissolved organic carbon and total dissolved nitrogen analysis. Int J Environ Anal Chem 2007;87(6):387–99.

21. Gershey RM, MacKinnon MD, Williams Pj, Moore RM. Comparison of three oxidation methods used for the analyis of the dissolved organic carbon in seawater. Mar Chem. 1979;7(17361):289–306.

22. David W. Menzell; Ralph F. Vaccaro. The Measurement of dissolved organic and particulate carbon in seawater. Woods Hole Oceanogr Jnstitution, Woods Hole, Massachusetts. :138–42.

23. Manfred Ehrhardt. A new method for the automatic measurement of dissolved organic carbon in sea water. Deep Sea Res. 1969;16.

24. Collins KJ, Le PJ, Williams B. An automated photochemical method for the determination of dissolved organic carbon in sea and estuarine waters. Mar Chem. 1977;5(2):123–41.

25. Wangersky PJ. The determination of dissolved organic carbon in sea water. 1981; 28–30.

26. Gordon DC, Sutcliffe WH. A new dry combustion method for the simultaneous determination of total organic carbon and nitrogen in seawater. Mar Chem. 1973;1(3):231–44.

27. Sharp JH. Total organic carbon in seawater - comparison of measurements using persulfate oxidation and high temperature combustion. Mar Chem. 1973;1(3):211–29.

28. Sugimura Y, Suzuki Y. A high-temperature catalytic oxidation method for the determination of non-volatile dissolved organic carbon in seawater by direct injection of a liquid sample. Mar Chem. 1988;24(2):105–31.

29. De Baar HJW, Brusaard C, Hegeman J, Schijf J, Stoll MHC. Sea-trails of three different methods for measuring non-volatile dissolved organic carbon in seawater during hte JGOFS North Atlantic pilot study. Mar Chem. 1993;41:145–52.

30. Williams PM, Druffel ERM. Dissolved organic matter in the ocean: Comments on a controversy. Oceanography. 1988;1:14–7.

31. Koprivnjak JF, Blanchette JG, Bourbonniere RA, Clair TA, Heyes A, Lum KR, et al. The underestimation of concentrations of dissolved organic carbon in freshwaters. Water Res. 1995;29(1):91–4.

32. Williams PM. Measurement of dissolved organic carbon and nitrogen in natural waters. Oceanography. 1992;5(2):107–16.

33. Thomas C, Cauwet G, Minster J-F. Dissolved organic carbon in the equatorial Atlantic Ocean. Mar Chem. 1995;49(2–3):155–69.

34. Cauwet G. Automatic determination of dissolved organic carbon in seawater in the sub-ppm range. Mar Chem. 1984;14(4):297–306.

35. McKenna JH, Doering PH. Measurement of dissolved organic carbon by wet chemical oxidation with persulfate: influence of chloride concentration and reagent volume. Mar Chem. 1995;48(2):109–14.

36. MacKinnon MD. A dry oxidation method for the analysis of the TOC in seawater. Mar Chem. 1978;7(1):17–37.

37. Hedges JI, Bergamaschi BA, Benner R. Comparative analyses of DOC and DON in natural waters. Mar Chem. 1993;41(1–3):121–34.

38. Koshy K, Mataki M. Photochemical Oxidation and Flow Injection Conductivity Determination of Dissolved Organic Carbon in Estuarine and Coastal. 2000;12:157–63.

39. Lopes CB, Abreu S, Válega M, Duarte RMBO, Pereira ME, Duarte a. C. The Assembling and Application of an Automated Segmented Flow Analyzer for the Determination of Dissolved Organic Carbon Based on UV-Persulphate Oxidation. Anal Lett. 2007;39(9):1979–92.

40. Das SS, Patawari BK, Patowari PK, Halder S. Computational Analysis for Mixing of Fluids Flowing through Micro- Channels of Different Geometries. 2014;(Aimtdr):1–6.

Attachments

A. COMSOL Multiphysics 5.0 simulations

Steps followed to program simulations of chapter 3:

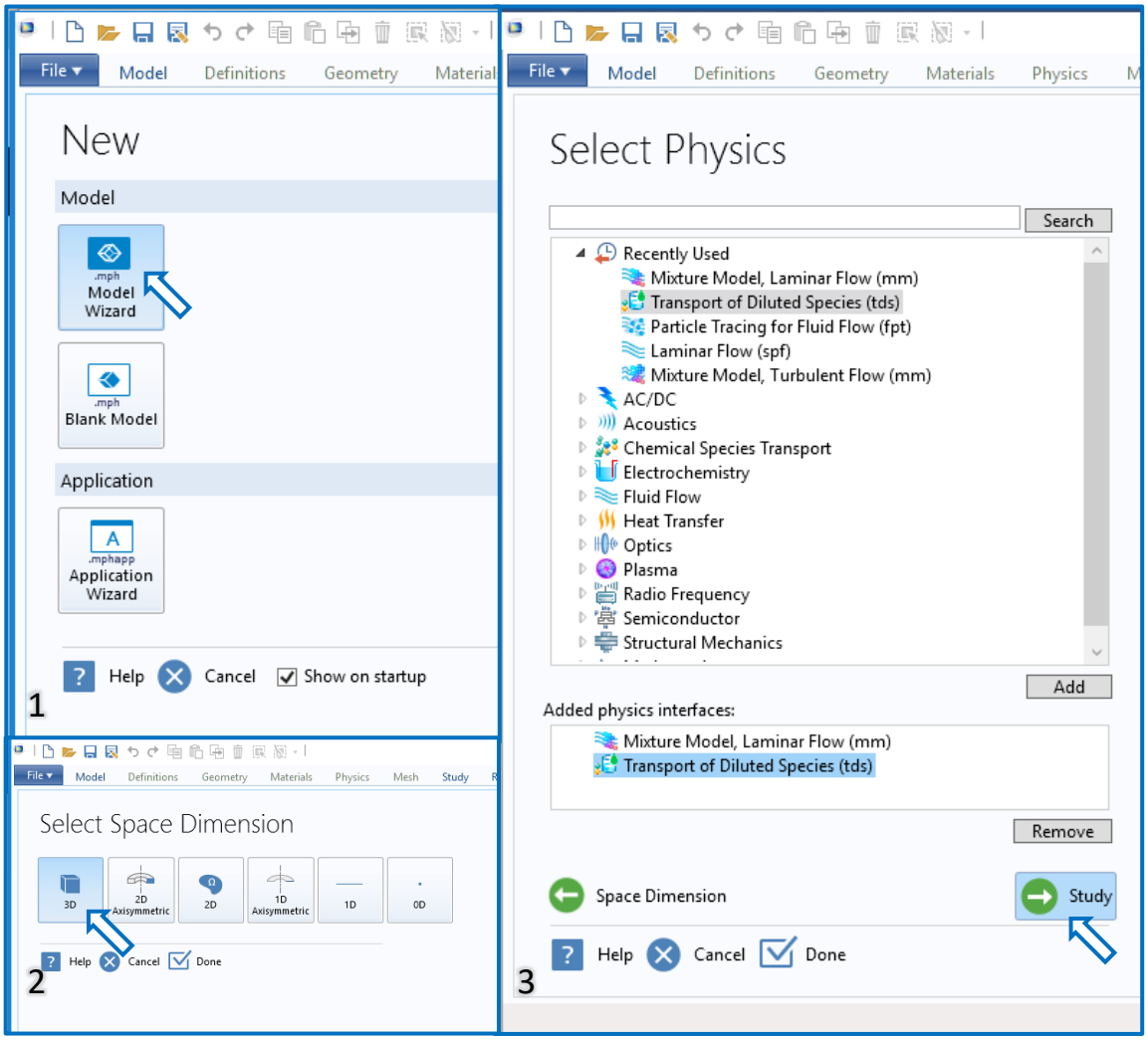

Figure 42 Preparing COMSOL Multiphysics 5.0 simulation: step 1) Select "Model Wizard"; step 2) Select "3D"; step 3) Select "Mixture Model, Laminar Flow (mm)" and "Transport od Diluted Species (tds)" then select "Study"

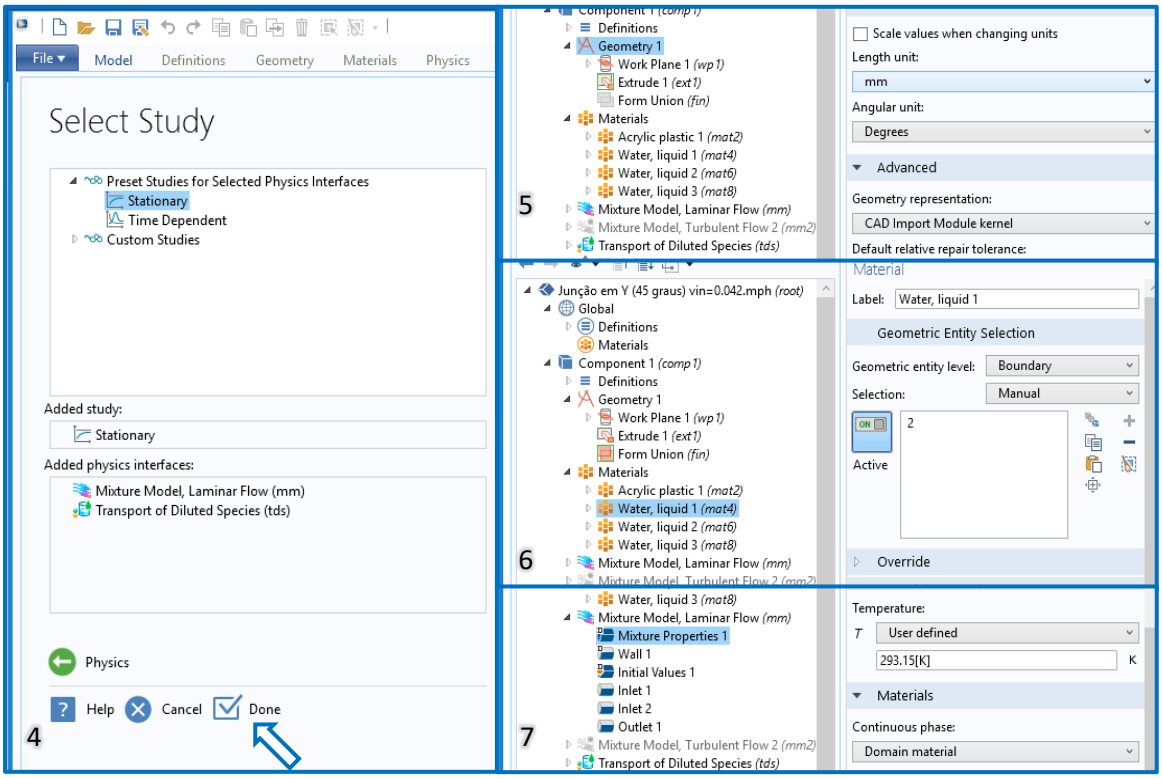

Figure 43 Preparing COMSOL Multiphysics 5.0 simulation: step 4)Select "Stationary" then select "Done"; step 5) In the geometry section change length unit to "mm", then introduce the geometry; step 6) In the Material section, add 1 material of "Acrylic plastic" for the walls of the geometry and 3 materials of "Water, liquid", one for the domain and two for each inlet; step 7) On the "Mixture Model, Laminar flow" section, select "Mixture properties" and define Temperature as 293.15 K (20°C)

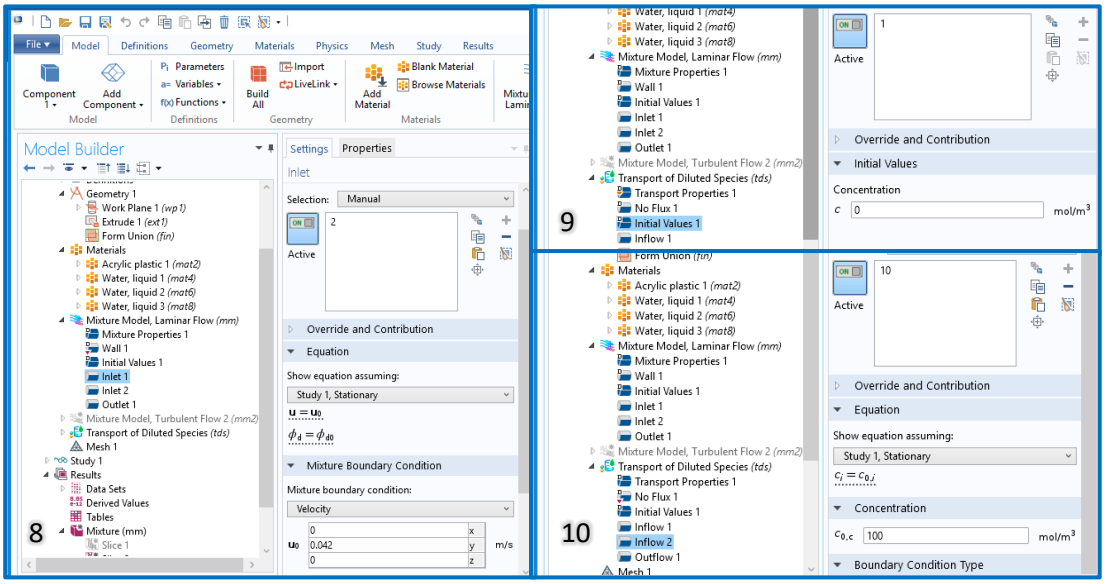

Figure 44 Preparing COMSOL Multiphysics 5.0 simulation: step 8) On the "Mixture Model, Laminar flow "section choose which surfaces are Walls, Inlet 1, Inlet 2 and Outlet; step 9) On the "Transport of Diluted Species" section specify in "Initial Values" original concentration as 0 mol/m^3; step 10)) On the "Transport of Diluted Species" section choose which surfaces are Walls, Inlet 1, Inlet 2 and Outlet, and choose concentration of Inlet 1 as 0 mol/m^3 and Inlet 2 as 100 mol/m^3

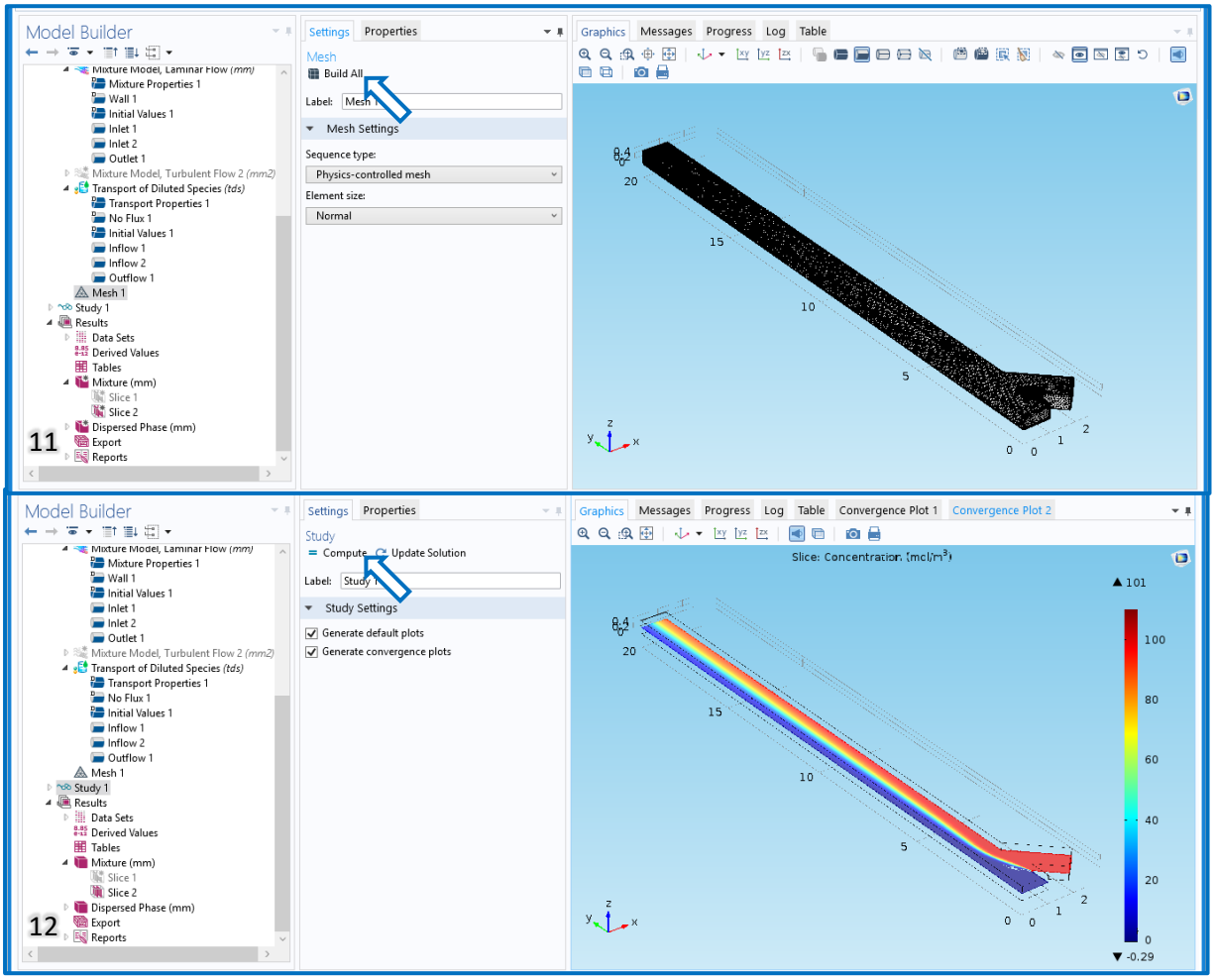

Figure 45 Preparing COMSOL Multiphysics 5.0 simulation: step 11) In the "Mesh section" select normal in element size and them "Build all"; step 12) In the "Study" section select compile

B. Results of Experimental Testing of Generation-1 Short Mesochannels (ShM)

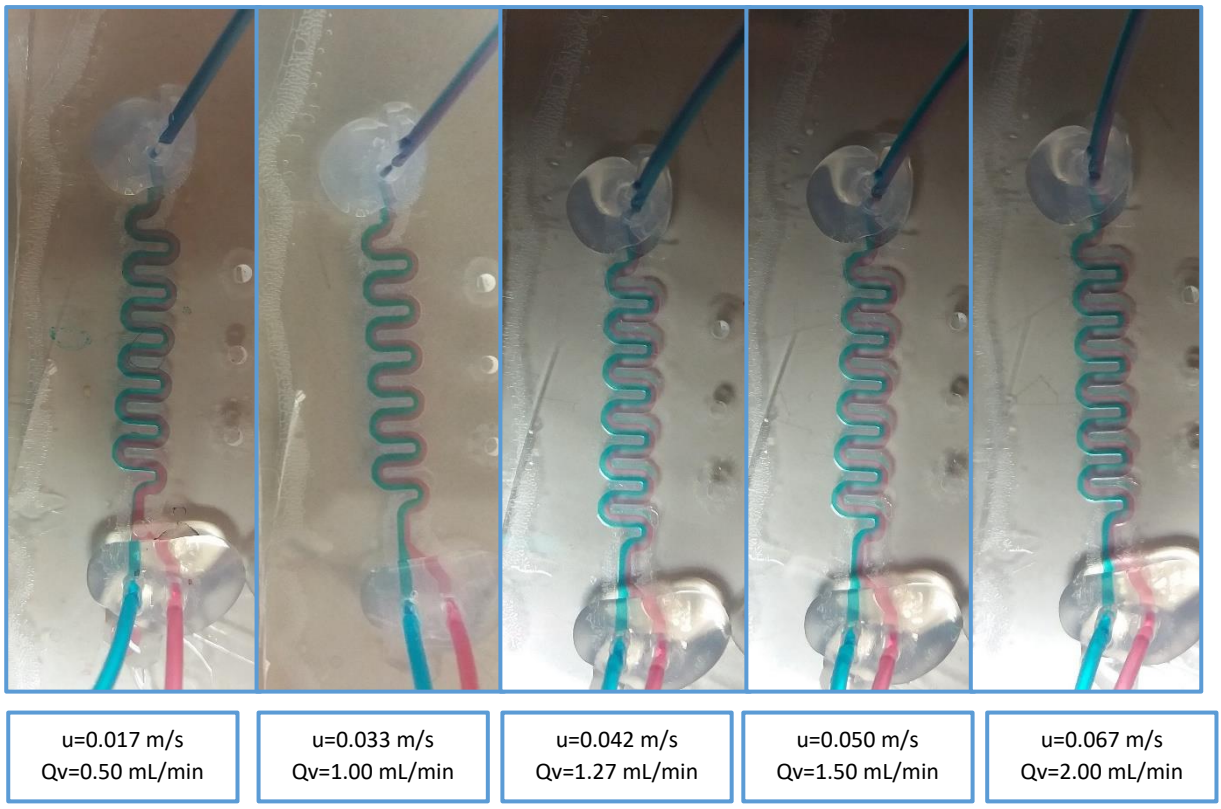

Figure 50 Photos of the experimental testing of ShM mesochannles later analysed through the RGB profiler option of the program ImageJ

C. Results of Experimental Testing of Generation-1 S-shaped Mesochannels (SM)

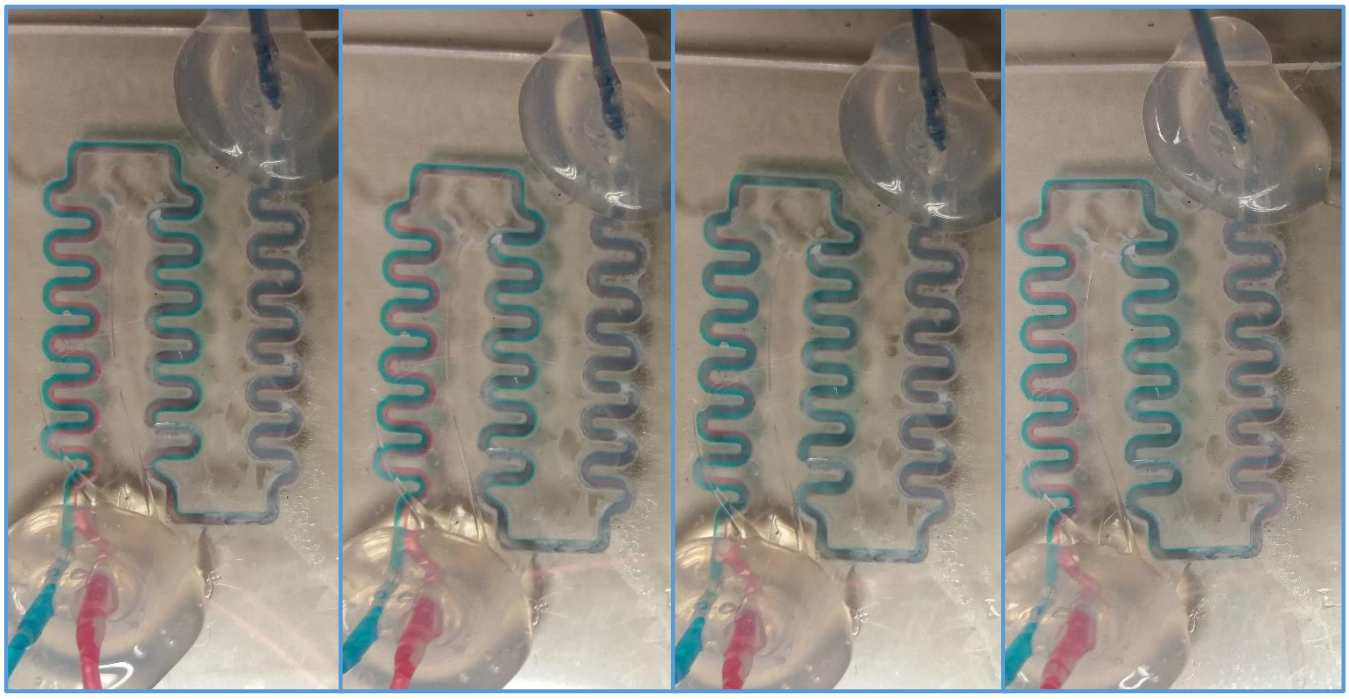

u=0.017 m/s
Qv=0.50 mL/min

u=0.033 m/s
Qv=1.00 mL/min

u=0.042 m/s
Qv=1.27 mL/min

u=0.050 m/s
Qv=1.50 mL/min

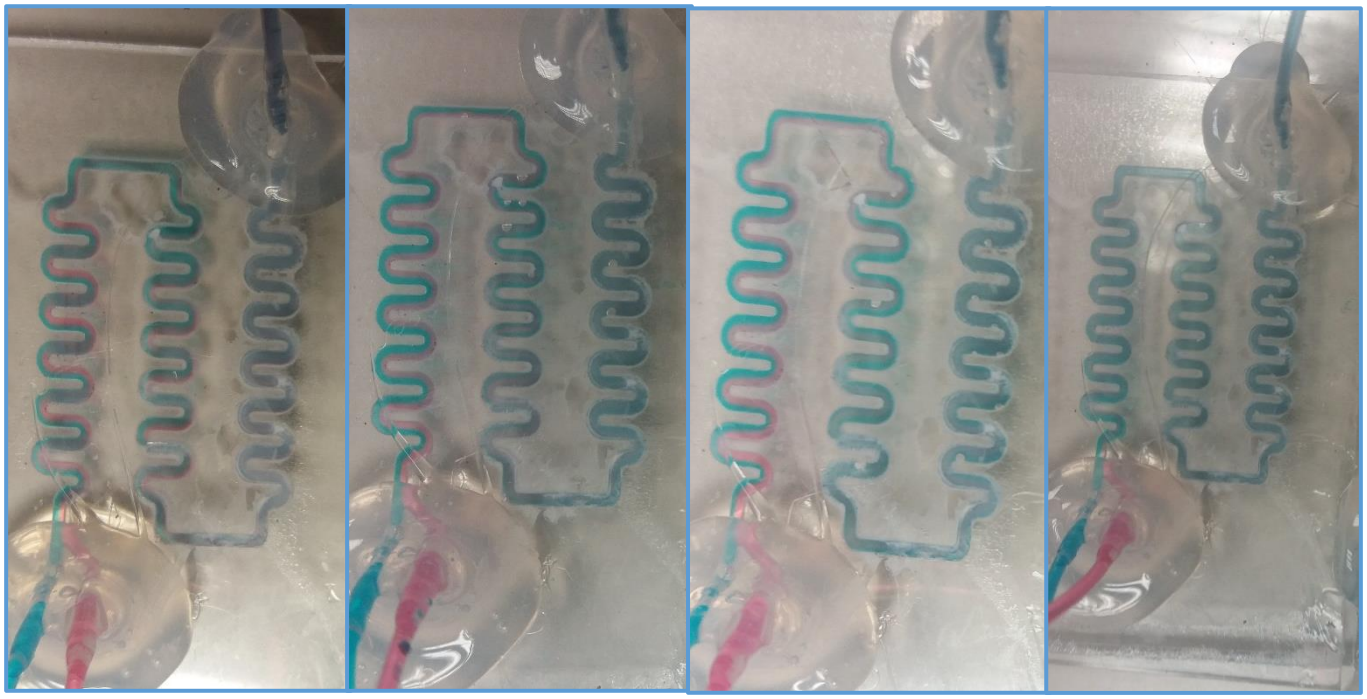

u=0.067 m/s
Qv=2.00 mL/min

u=0.100 m/s
Qv=3.00 mL/min

u=0.133 m/s
Qv=4.00 mL/min

u=0.167 m/s
Qv=5.00 mL/min

Figure 56 Photos of the experimental testing of SM mesochannles later analysed through the RGB profiler option of the program ImageJ

D. Results of Experimental Testing of Generation-1 Long Mesochannels (LM)

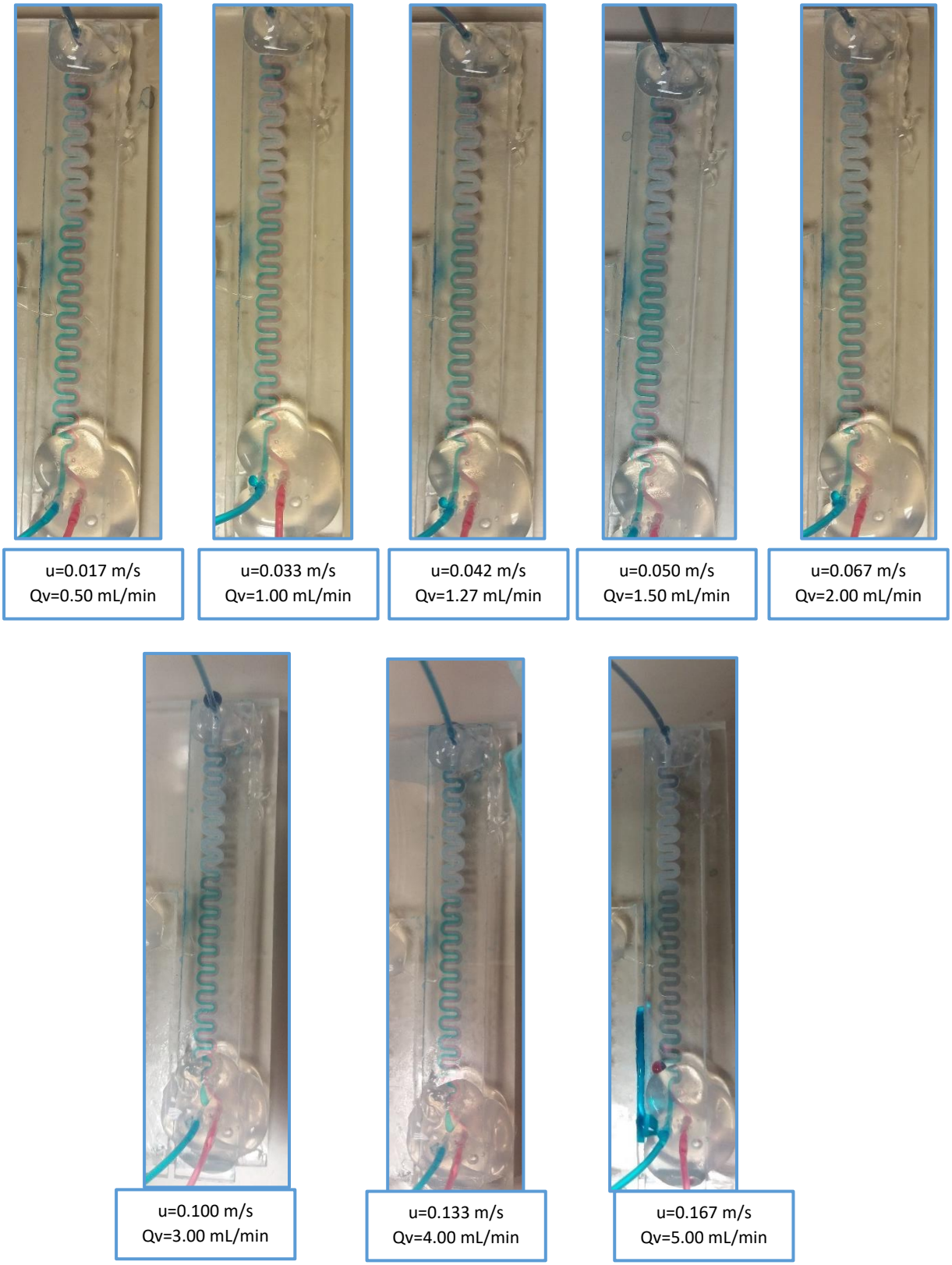

Figure 57 Photos of the experimental testing of LM mesochannles later analysed through the RGB profiler option of the program ImageJ